Adsorption and Transport Mechanisms of Virus-like Particles on Ion Exchangers

Patrícia Pereira Aguilar

Marshall Plan Scholarship Paper

Research stay at the Bioseparations Engineering Laboratory of Professor Giorgio Carta at the University of Virginia (3rd April – 3rd October 2017)

Marshallplan-Jubiläumsstiftung
Austrian Marshall Plan Foundation

Table of Contents

1 Project Overview

Virus-Like Particles (VLPs) are self-assembled protein structures that mimic native viruses. As the virus that they mimic, VLPs have the ability to stimulate humoral and cellular immune responses. Besides that, since they completely lack the viral genetic material, they have the inability to replicate or proliferate, turning them into a safe alternative for conventional vaccines. Those characteristics together turn VLPs into key candidates for modern vaccines and drug delivery systems. All manufacturing processes of biopharmaceuticals, especially those that aim to be used in gene therapy applications, require high purity levels. Currently, despite the already achieved improvements in VLPs manufacturing regarding cell engineering and upstream production, the downstream processing is lagging behind. Complex, time-consuming and low productivity methods are still used as purification strategies. Density gradient centrifugation and ultrafiltration are the pharmaceutical industry standard techniques. Along with their low yields, the scale-up of these methods is too complex or, in some cases, not possible. The upstream optimization of large-scale VLP production rapidly increased the demand for new, fast, cost efficient and scalable purification strategies and/or unit operations. In biotechnological and pharmaceutical industries, the majority of the purification strategies include or are exclusively dependent on chromatographic bioseparations. At present, anion exchange chromatography is a well-established technique for the purification of many biomolecules, such as proteins and DNA. Charged hydrogels and/or chromatography beads in form of polymer-grafted media are known to have very high protein binding capacities and to be able to bind large molecules such as plasmids and viruses. However, for large biomolecules the separation mechanisms are still not clear. This lack of knowledge largely hinders process development and optimization. Thus, understanding the underpinnings of the chromatographic methods used in the downstream processing of large biomolecules, such as VLPs, is fundamental for the development of more robust and economical processes. Consequently, the aim of my doctoral project is to elucidate how VLPs, large proteins and protein superstructures partition into highly charged hydrogels and polymer-grafted media. Experimental and theoretical approaches will be used to access the binding equilibrium and mass transfer properties of large biomolecules on porous media. The binding equilibrium will be accessed through adsorption isotherms and binding and elution chromatographic studies. The uptake kinetics will be studied with conventional batch uptake experiments and will be followed microscopically using confocal laser scanning microscopy (CLSM) and transmission electron microscopy (TEM). Besides that, a mathematical model of the mass transfer properties will be developed and the output will be compared with the experimental results. In the end, a mechanistic

understanding of the VLPs chromatographic purification is expected and we hope that our findings will assist in the development of more robust and economical purification processes for VLPs, which are current important candidates for new vaccines.

This report aims to present the part of my doctoral work that was developed during the Research stay at the Bioseparations Engineering Laboratory of Professor Giorgio Carta at the University of Virginia (USA).

2 Introduction

2.1 Virus-like particles (VLPs)

Virus-like Particle (VLP) technology aims to reproduce the immuno-stimulatory properties of viruses while omitting their infectious abilities. It has been shown that VLPs are safe and highly efficacious in humans [1–4] In general terms, VLPs are recombinant highly ordered repetitive nanostructures, consisting of one or several viral proteins (Figure 1). As their native viruses, some VLPs also contain an external lipid envelope derived from the host cell membrane (Figure 1 – Enveloped VLPs). On one hand, these structural arrangements provide VLPs their ability to stimulate both humoral and cellular immune responses. On the other hand, VLPs completely lack viral genomic material being unable to replicate or proliferate.

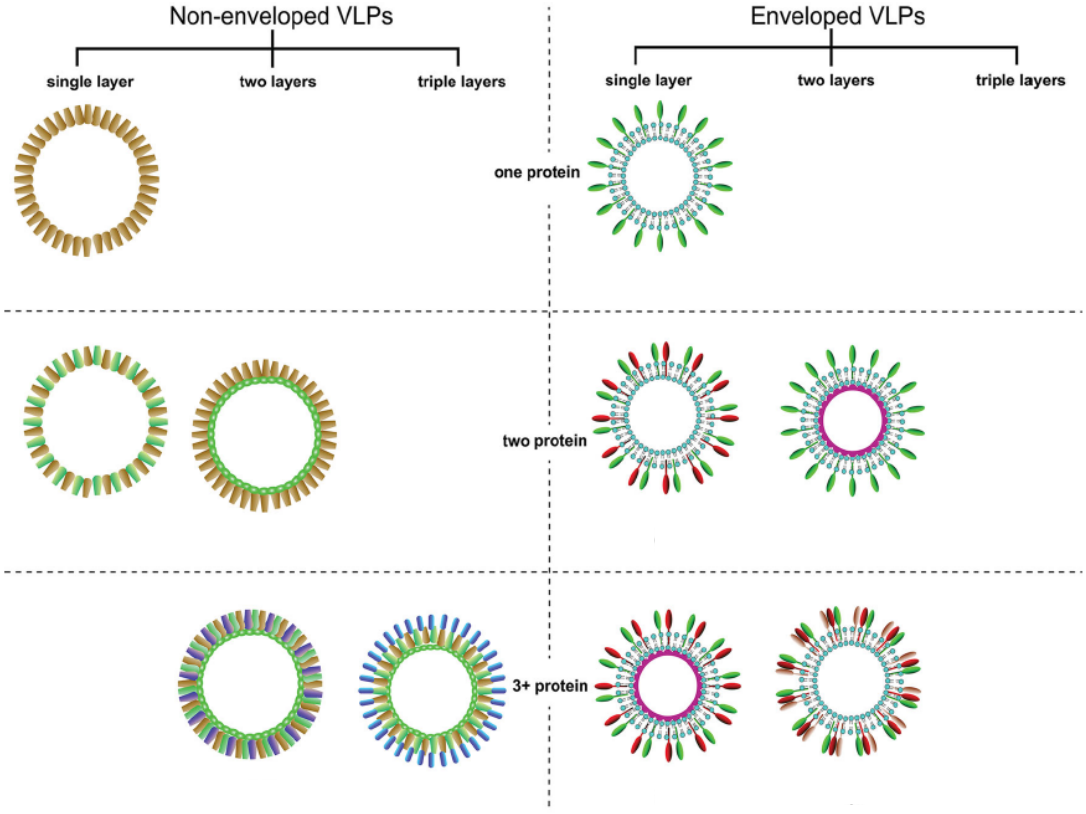

Figure 1. Structural diversity of VLPs. Both capsid-based and enveloped VLPs can be single or multi-layered and composed of single or multiple proteins (adapted from [5]).

As non-infectious biomolecules, VLPs are safe not only for the recipients at the administration level, but also for the operators during the entire manufacturing process, avoiding the risk of accidental infections. Due to their characteristics, VLPs were primarily used as vaccines designed to prevent infectious diseases. However, VLP applications have been extended to drug delivery, gene therapy and cancer treatment [5]. Consequently, the interest in VLP technology has increased in recent years (Figure 2).

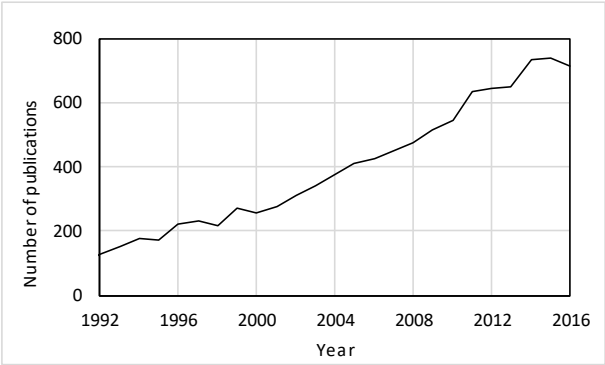

Figure 2. Increase in the interest in virus-like particle technology. Total number of publications from Scopus when searching for “virus like particles” in the field: article title, abstract and keywords.

2.2 VLP production

Virus-like particles (VLPs) are produced by recombinant expression of one or several viral proteins. Several expression systems have been successfully used for VLP production, including bacteria, yeast, insect cells, mammalian cells and plants [1,3,6–12]. The choice of the expression system primarily relies on the requirements for protein folding and post-translational modifications. Additionally, the structural complexity of the VLP also defines the required complexity of the expression system. Lastly, the cost-effectiveness of the production platform is also taken into account [1,2,4].

The most advantageous expression systems in terms of cost-effectiveness and scalability are bacteria and yeast. For non-enveloped VLPs with one or two structural proteins, bacteria expression systems are able to produce the viral proteins with high yields at low cost [13]. However, bacteria are unable to perform mammalian-like post-translational modifications, which can lead to poor immunogenicity of the VLPs [12].

A more complex platform is the Baculovirus/insect cell (B/IC) expression system. In this case, the viral proteins are encoded in the genome of a Baculovirus, which is later used to infect the insect cells

where the VLPs will be produced. Since Baculovirus engineering is a fast and easy process, this system is suitable for the production of vaccines against viruses with high mutation rate such as influenza viruses [6]. The yields in protein production of the B/IC system are comparable to the yields in bacteria and yeast with the advantage that insect cells have the capability of producing post-translational modifications of higher complexity. However, simultaneously to the VLP production the insect cells co-produce enveloped Baculovirus particles, which turns purification into a challenging and expensive process [7].

Transgenic plants, such as *Nicotiana tabacum* and *Arabidopsis thaliana*, have also been used as expression systems for VLP production. Plant cells are usually transformed through *Agrobacterium tumefaciens* infection, leading to nuclear integration of the gene of interest in the host genome [8]. Current plant expression systems have the ability to perform mammalian-like post-translational modifications and are highly scalable and safe. The high flexibility and speed of plant expression systems is one of their main advantages. However, there are still important technical and regulatory challenges to overcome before plants can be used at commercial scale. For example, the downstream processing of plant-based materials from whole plants is complex and time consuming. Plants produce more cell debris than other expression systems, making the clarification of plant extracts difficult and impossible to achieve by a single filtration step (as in the case of mammalian cells). Moreover, direct loading of plant extracts onto chromatography resins usually leads to rapid resin fouling. Therefore, new downstream processing strategies are necessary to fulfil the needs of VLP production in plants [9].

Mammalian cell expression systems have the capacity of producing complex proteins with accurate post-translational modifications [10]. Despite of their lower productivities when compared to other systems, mammalian cells are favourable due to their capability of producing VLPs with the required post-translational modifications and authentic assembly. In enveloped VLP production, the main drawback of this system is that along with the VLPs, mammalian cells secrete other particles, such as microvesicles and exosomes. Both, VLPs and cellular vesicles, contain an outer membrane derived from the host cell membrane. Consequently, VLPs and vesicles are chemically and fiscally similar, making their separation a difficult and expensive process [14,15]. Yet, mammalian cells are typically used to produce complex enveloped VLPs containing multiple structural proteins with reasonable productivities. When transient transfection is used, VLPs can be harvested in approximately 48 to 72 h post transfection [11]. Chinese Hamster Ovary (CHO) cell lines are one of the most used mammalian cell systems for VLP production. When compared with other mammalian cells, this system has the

advantage of presenting a lower risk of contamination by human viruses because they are not human-derived. Table 2.1 summarizes the main advantages and disadvantages of the VLP expression systems.

Table 2.1. Comparison of VLP expression systems (adapted from [12]).

Expression system	Advantages	Disadvantages
Bacteria	Less expensive; simplicity of expression; fast growth rate; high-level expression; genetic stability; simple process scale-up	Lack mammalian-like PTM; Poor ability on immunogenicity; Presence of host cell-derived contaminants
Yeast	Less expensive; high-density fermentation; modification of the expression protein; moderately rapid expression; support most protein folding and PTM	High mannose modification; some secretory proteins cannot get ideal results; enhanced safety precautions are required
Insect cells	Moderately rapid expression; support most protein folding and eukaryotic-type PTM of the expression protein; works well for non-enveloped and enveloped VLPs, free of mammalian pathogens	High cost; difficult to scale-up; incomplete modification of proteins; low-level expression, contamination of product with enveloped baculovirus particles; perform simpler N-glycosylation compared to mammalian cells
Mammalian cells	Perform appropriate complex mammalian-type PTMs; perform authentic assembly and folding of recombinant proteins; works well for non-enveloped and enveloped VLPs	High cost; difficult to scale-up; lengthy expression time; low yield; vulnerable to infection with mammalian pathogens
Plants	Rapid expression; highly scalable; less expensive; free of mammalian pathogens; support most protein folding and eukaryotic-type PTM	Low yield; technical and regulatory issues

2.3 VLP downstream processing (DSP)

In general, the ultimate goal of downstream processing is the recovery and purification of biological products from process- and product-related impurities. At the end, it is expected to obtain a product with high purity, potency and quality that meets the guidelines of the regulatory agencies such as Food and Drug Administration (FDA) and European Diagnostic Manufacturers Association (EDMA). Process-related impurities are mainly derived from the host cell (e.g., cells and cell debris, host cell proteins - HCPs, DNA, endotoxins, polysaccharides and lipids), the upstream processing (e.g., culture media components, anti-foam agents and additives, such as antibiotics) and the downstream processing (e.g., leachables in chromatography, tags, stabilizers, excipients, proteases and nucleases).

Product-related contaminants in VLP manufacturing result from product alterations during up- and downstream processing (e.g., aggregates, misfolded, deformed and disassembled particles or subunits) [16–18]. Additionally, in the specific case of enveloped VLPs, the secretion of vesicles by certain types of host cells increases the challenge in the separation processes because both, vesicles and VLPs, contain a similar outer membrane derived from the host cell [14,15].

Virus like particles are complex bio-nanoparticles with a wide range of sizes, shapes, compositions and surface structures. The VLP surface composition defines its physicochemical properties, including isoelectric point (pI), hydrophobicity and charge distribution. Together, VLP surface composition and size delineate the options for downstream processing methods. Moreover, the high complexity of these bio-nanoparticles requires a combination of advanced analytical techniques for the in-process product purity and quality control [2,19–22].

In general, a downstream processing strategy for bio-nanoparticles such as viruses, viral vectors or VLPs involves several unit operation as represented in Figure 3.

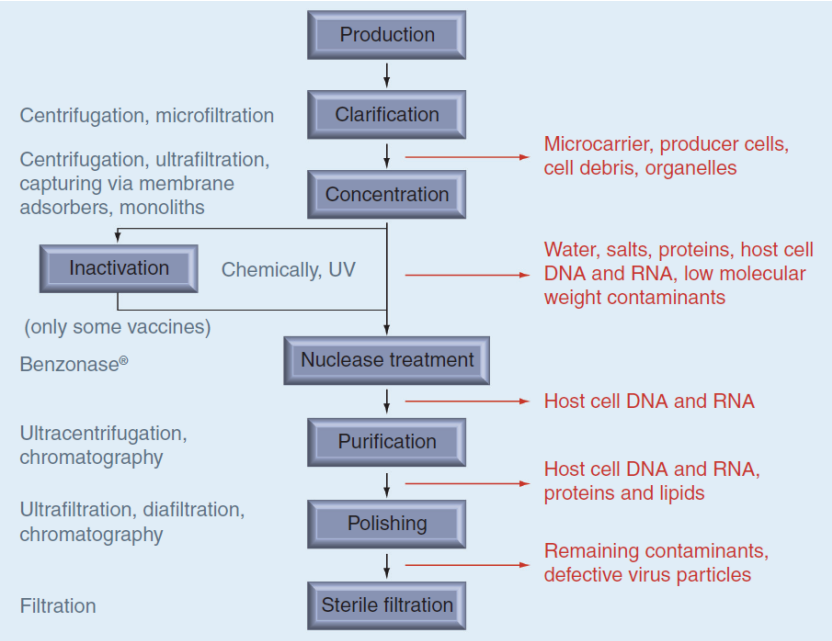

Figure 3. Generic flowchart of downstream processes for bio-nanoparticles such as viruses, viral vectors and VLPs for pharmaceutical application as vaccines or gene therapy vehicles (from [17]).

The downstream processing of a VLP product starts with the clarification step. At this point, solid-liquid separation of the cell culture broth is achieved by means of centrifugation or filtration techniques. Specifically, this step aims to remove cells, cell debris and insoluble aggregates.

Depending on the host and viral protein(s), VLPs can be produced intra- or extracellularly. When VLPs are not secreted to the extracellular medium, a cell lysis step is required before the clarification step. At large scale, cell lysis for VLP recovery is usually performed using high-pressure homogenization [23,24].

Centrifugation is one of the most commonly used unit operations to clarify cell culture bulks at laboratory scale. At industrial scale, the choice tended to be continuous flow centrifugation [25]. However, the required high investment costs and the scalability problem from laboratory to pilot or production scale are some of the main drawbacks of this technology. Additionally, the trend for using cleaning- and validation-free disposable technologies in the biopharmaceuticals manufacturing processes lead to the development and use of new membrane technologies such as dead-end or tangential flow filtration [26,27]. Membrane processes are scalable methods that can be easily operated under good manufacturing practice (GMP), being often selected for the clarification step of many biopharmaceuticals including VLPs [16,18]. Despite membranes with pore sizes in the range of 0.45-1 µm are used, the main drawback of this technique is the risk of VLP losses mainly due to mechanical disruption, exclusion of higher diameter particles, unspecific VLP adsorption to the membrane surface or pore obstruction [17].

After clarification, an efficient capture/concentration step should allow the reduction of the bulk volume in order to concentrate the product 10-100 times prior to further purification techniques [16]. Furthermore, during the concentration step, a buffer exchange can be performed. The most commonly used unit operations for the concentration step in VLP production are filtration (ultra- and diafiltration), precipitation (using ammonium sulfate or polyethylene glycol as precipitation agents), extraction (aqueous two-phase systems) and chromatography (affinity, ion exchange, hydrophobic interaction and mixed mode) [16–18,22,28].

Ultra- and diafiltration techniques aim to reject the product of interest (VLP) concentrating it in the retentate and simultaneously allowing small impurities and water to cross to the permeate side. The main advantages of these techniques are their high-throughput combined with the simultaneous capability of product concentration and partial purification based only on the size differences between VLPs and impurities. This allows the creation of a platform that can be used across different VLPs [29]. Nevertheless, the resulting product from this step still requires further purification to separate all remaining impurities with similar molecular weights.

Other techniques widely used in the capture/concentration step of many biopharmaceuticals are precipitation and flocculation. However, these techniques have been less explored in the downstream

processing of VLPs due to the risk of irreversible aggregation and product alterations as well as co-precipitation of other large biomolecules such as nucleic acids [30].

The most common method for the concentration and/or purification of macromolecules, such as VLPs, is density gradient centrifugation. Sucrose, caesium chloride (CsCl) or iodixanol gradients are well known and typically used to purify small amounts of bulk for preclinical studies [16,17]. The separation of bio-nanoparticles according to their distinctive densities is the basic principle of gradient centrifugation. The main advantage of this technique is the possibility of combining both, concentration and purification steps, in a single unit operation. Moreover, this method allows the separation of empty and full particles with reasonable resolution [17]. However, the laborious and expensive scale-up plus the need to remove the additives in an extra purification step are the two main drawback of this technique, which explain the preference for chromatographic separation techniques during the VLP downstream processing at large scale.

Chromatography is the most commonly used unit operation for large-scale capture, concentration and purification of biopharmaceuticals. The chromatographic separation relies on the selective physicochemical interactions between the product of interest and the impurities with the stationary phase [31]. For achieving a successful chromatographic purification several points have to be considered in order to fit the requirements dictated by the properties of the product of interest. Physical structure and surface chemistry of the stationary phase, composition of the mobile phase, mode of operation and system hardware are some of the parameters that need to be considered. Packed beds (beads), monoliths and membrane adsorbers are well known chromatographic structures (Figure 4) and all of them have been used as stationary phases in VLP capture/purification [14,15,17].

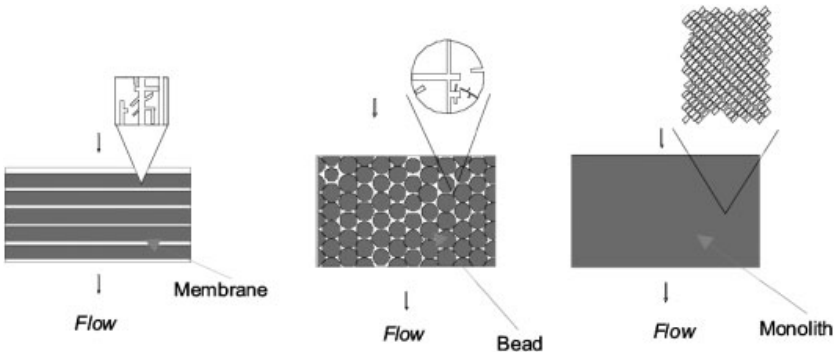

Figure 4. Comparison between membrane adsorbers, packed beads and monoliths for biopharmaceuticals purification (from: [31]).

The matrix of packed beds consists of resin beads packed into a column. Polymer or inorganic materials can be used to produce chromatographic resins. Polymer-based beads consist of either natural polymers such as agarose, cellulose and dextran or synthetic polymers as polyacrylamide and polymethacrylate. Inorganic beads are usually made of hydroxyapatite, silica or porous glass. Beads can be spherical or non-spherical and are available as porous, non-porous or solid-core resins (Figure 5). The pore size in a conventional porous resin usually varies between 10 and 100 nm, although in the past years there were also developed macro-porous resins with pore diameters up to 400 nm [31].

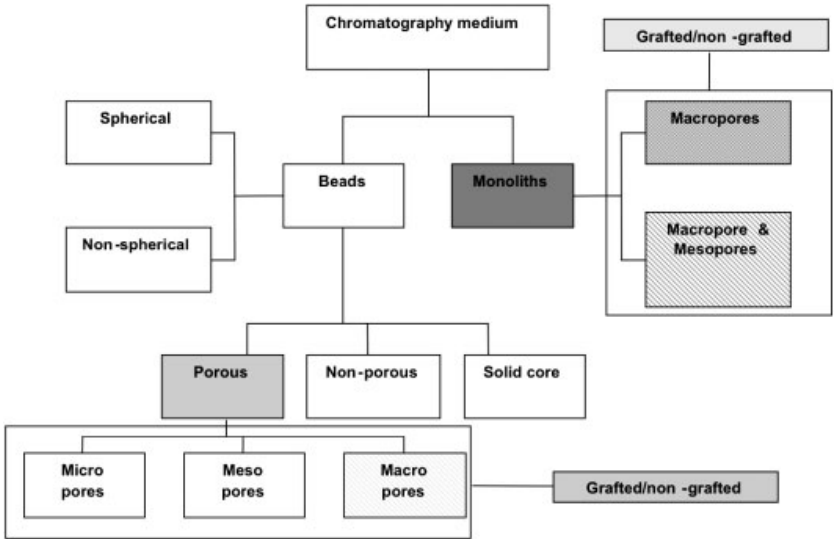

Figure 5. Categories of Chromatographic media according to their physical properties (from: [31]).

Due to the large diameter of virus particles (30-300 nm), the mass transfer during the chromatographic capture/purification of VLPs using packed beds is limited by pore-diffusion or pore-exclusion effects. Even small virus particles, which are able to diffuse into large pores, present a two- to 100-fold slower diffusion than smaller biomolecules [17]. Thus, at usual processing times, VLPs adsorb mainly to the outer surface of the beads, resulting in lower dynamic binding capacities when compared other biopharmaceuticals such as proteins.

Convective chromatography matrices, such as monoliths and membrane adsorbers, have the advantage over packed bead matrices of offering nearly no diffusion limitations and high dynamic capacities. Monoliths are continuous stationary phases formed *in situ* creating a network of pores or channels allowing convective flow of the mobile phase through the entire matrix [32]. Despite their large capacity (high surface area) and high resolution, monoliths have shown to be prone to clogging especially when high amounts of host cell DNA are present in the column. Moreover, since both

product of interest and impurities can access all binding sites there is the risk of binding competition or displacement of the product of interest by the impurities.

Membrane adsorbers for biopharmaceuticals purifications can be found in the form of flat sheets, hollow fibers and radial-flow devices. Due to the high surface area of the different setups and the cross-flow principle, membrane adsorbers usually present high binding capacities and reduced particle accumulation near the pore entrance. However, the breakthrough of the product of interest is generally broadened, leading to poor utilization of the total surface area available. Furthermore, the product of interest is usually diluted and gradient elutions are very challenging [17].

The different surface chemistries of the chromatographic matrices allow several different interaction principles in chromatography. Currently several modes of chromatographic separations can be used for the purification of bio-nanoparticles, including size-exclusion chromatography (SEC), ion exchange chromatography (IEC), affinity chromatography (AC), hydrophobic interaction chromatography (HIC) and mixed-mode chromatography [16–18].

The most attractive purification method is affinity chromatography (AC), because it allows the separation of most of the contaminants in a single step, due to its high selectivity. However, this type of chromatography requires extensive investigation to find a unique antibody with high selectivity or the introduction of a tag in the product of interest, which has to be later removed in another purification step. These two drawbacks result in high process costs and difficult the establishment of a platform downstream process.

Size exclusion chromatography (SEC) is based on the partitioning of the biomolecules along the chromatographic column. This type of chromatography relies exclusively on the size difference between the product of interest and the impurities, allowing the maintenance of optimal conditions for the product of interest. However, the main drawbacks are the low capacity, product dilution and the poor pressure resistance of the matrix, requiring low flow rates and reducing the productivity. Nevertheless, SEC is still applied in most of the cases as a final polishing step in VLP manufacturing [16–18].

In hydrophobic interaction chromatography (HIC) the separation depends on the differential interaction between the hydrophobic ligands on surface of the chromatographic matrix and the hydrophobic groups present on the product and impurities surfaces. To enhance the hydrophobic interactions, during HIC the samples are loaded onto the chromatographic columns under high salt concentrations (usually using kosmotropic salts). The application of high salt concentrations leads to an increased risk in VLP aggregation and consequently product loss [14]. To overcome this, mixed

mode chromatography simultaneously combines ionic interactions, hydrogen bounds and/or hydrophobic interactions allowing VLPs to bind under less harmful conditions and minimizing product loss.

Ion exchange chromatography (IEC) is the most prevalent method for purification of biopharmaceuticals at laboratory and industrial scale [18]. IEC separations are based on the ionic interactions between the charged ligands on the surface of the chromatographic matrix and the surface charges on the product and impurities surfaces. In positive-mode applications, the product of interest is bound to the column, while most of the impurities are collected in the flowthrough. Due to the differences in surface charge of different biomolecules, the bound product can be separated from the bound impurities by linearly increasing the ionic strength of the mobile phase and consequently weakening the binding strength.

In summary, the current downstream processing of virus like particles combines several individual unit operations that were primarily developed for smaller biomolecules such as proteins. The combined knowledge obtained from virus, viral vectors and VLPs current manufacturing processes reveals that there is still a lack of straightforward ready-to-use platforms for downstream processing of VLPs. Moreover, process development of VLPs is often delayed by the need to use a combination of laborious-intense offline analytical methods, such as gel electrophoresis, Western blotting, electron microscopy and nanoparticle tracking analysis. New technologies that allow the rapid control and characterization of the product are of high demand [16,18].

2.4 Human Immunodeficiency virus-like particles

An infective human immunodeficiency virus type 1 (HIV-1) is composed of two copies of the positive sense genomic viral RNA, cellular $tRNA^{Lys,3}$ molecules, the viral envelope (Env) protein, the Gag polyprotein, and the three viral enzymes: protease (PR), reverse transcriptase (RT), and integrase (IN) which are packaged as domains within the Gag-Pro-Pol polyprotein [33]. Conversely, the formation of HIV-1 VLPs simply requires the recombinant expression of the Gag polyprotein, without any other viral proteins or RNA [1,8,11,15,33–35]. As in the native virus, the HIV-1 gag VLP assembly is mediated by the Gag polyprotein, which binds to the host cell plasma membrane, makes the protein-protein interactions necessary to create spherical particles and recruits the host ESCRT (endosomal sorting complexes required for transport) machinery that promotes the budding event which releases the VLPs from the host cell. Figure 6 represents the native HIV-1 assembly, budding and maturation

processes, as well as the main components of the virus. The HIV-1 gag VLPs follow an assembly and budding process similar to the native virus, however there is no maturation phase due to the complete lack of the viral genome and viral enzymes that trigger the maturation process.

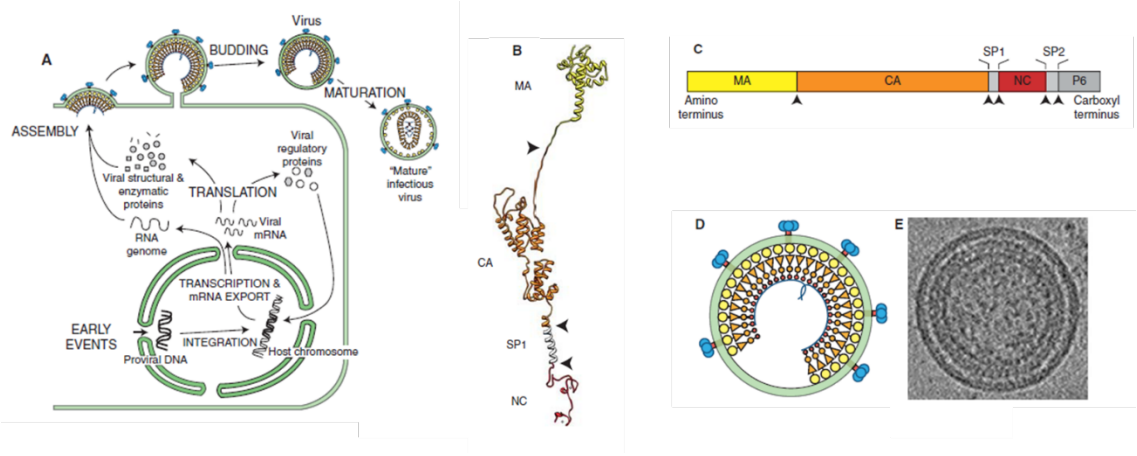

Figure 6. (A) Schematic illustration showing the different stages of HIV-1 assembly, budding, and maturation. (B) Structural model of the HIV-1 Gag protein. (C) Domain structure of the HIV-1 Gag protein. (D) Schematic model showing the organization of the immature HIV-1 virion. (E) Central section from a cryo-EM tomographic reconstruction of an immature HIV-1 virion (adapted from: [33]).

HIV-1 gag VLPs are spherical particles with diameters of about 100-150 nm and density around 1.18 g/cm^3 [15]. They are composed of approximately 2500 HIV-1 gag monomers, assembled on the inner surface of the particles (covering about 50% of the inner surface) and surrounded by a lipid bilayer derived from the host cell [35]. As for the native enveloped viruses, it is assumed that enveloped VLPs, such as HIV-1 gag VLPs, have multiple negative and positive charges distributed at their surface [36]. Therefore, it is reasonable to explore and design ion exchange based downstream processing methods such as ion exchange chromatography.

2.5 Adsorption and transport mechanism in ion exchange chromatography

Adsorption and transport mechanisms in chromatographic processes are primarily described by the equilibrium binding capacity and the adsorption kinetics. The equilibrium binding capacity refers to how much of the target biomolecule (and impurities) can be bound to the resin at equilibrium. The

adsorption kinetics determine the rate of the adsorption and therefore the residence time that will be later required to achieve an optimized purification in a chromatographic column [31].

In general, before adsorption takes place, biomolecules in the liquid phase encounter a series of resistances as represented in Figure 7. These transport resistances determine the adsorption rate and include: 1) External mass transfer in the fluid surrounding the particle; 2) pore diffusion in the liquid-filled intra-particle pores; 3) kinetic resistance to binding at the liquid-adsorbent phase interface and 4) solid or adsorbed phase diffusion.

The mass transfer resistances relevant for the adsorption and transport mechanisms evaluated in this work are explained in more detail in the "Results and Discussion" section of this report.

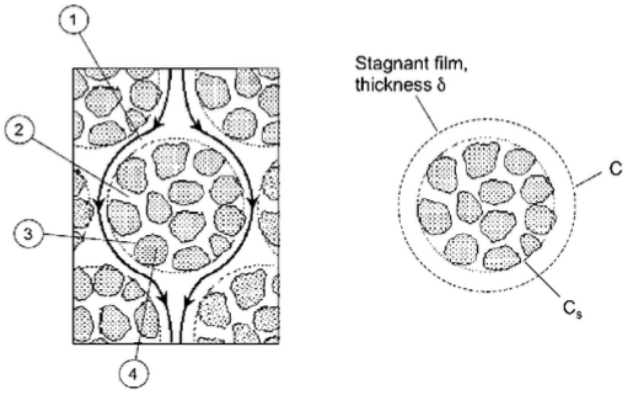

Figure 7. Location of transport and kinetic resistances to protein adsorption in porous particles. (1) External mass transfer; (2) pore diffusion; (3) kinetic resistance to binding; (4) solid or adsorbed phase diffusion. The sketch on the left shows particles in a packed bed with surrounding streamlines for mobile phase flow. The sketch on the right shows an approximation of the corresponding film model where external transport is represented by diffusion through a stagnant film (from: [31]).

3 Materials and Methods

3.1 Materials

3.1.1. Virus-like particles

Human Immunodeficiency Virus-like Particles (HIV-1 gag VLPs) were produced in Chinese Hamster Ovary (CHO) cells. The cell culture supernatant was provided by Icosagen (Tartumaa, Estonia). Briefly, a pQMCF vector containing the HIV-1 gag polyprotein gene under the control of the CMV promotor was transfected by electroporation into CHOEBNALT85 cells (6 x 10^6 cells, grown at 37°C). The plasmid-containing population was selected 48 h after transfection, by adding an aminoglycoside antibiotic (G418 Geneticin®, Gibco/Thermo Fischer, Waltham,MA) to the media. Ten days after selection, the cell culture temperature was dropped to 30°C and CHO CD Efficient FeedB (Thermo FisherScientific, Waltham, MA USA) was fed to the cell culture for 9 days. Western blot analysis detecting the HIV-1 p24 confirmed the production of HIV-1 gag VLPs. To obtain the cell culture supernatant, cells were removed by centrifugation (1000 g, 30 min). To avoid the growth of contaminants, 0.01% NaN_3 was added to the cell culture supernatant after centrifugation.

The HIV-1 gag VLPs were purified by preparative anion-exchange chromatography using a 8 mL CIMmultus QA monolith (BIA Separations, Ajdovščina, Slovenia) as described by Steppert et al [15]. Briefly, the purification runs were performed on an ÄKTA explorer 100 controlled by Unicorn software 5.10 (GE Health-care, Uppsala, Sweden). The mobile phases used were 50 mM HEPES, pH 7.2 (A) and 50 mM HEPES, 2 M NaCl, pH 7.2 (B). The flow rate was 5 mL/min. Before loading the clarified cell culture supernatant, the column was equilibrated with 15 column volumes (CV) of 50 mM HEPES, 350 mM NaCl, pH 7.2 (17.5% B). After the equilibrium phase, the column was loaded with 500 mL of 0.8 µm filtered CHO cell culture supernatant, followed by a 15 CV wash step (17.5% B). A three steps elution strategy was used at 38.1, 54.6 and 100% B with a hold of 15 CV for each step. During elution, 1 mL fractions were collected. VLPs eluted within the 54.6% B step were pooled, dialysed into 50 mM HEPES, pH 7.2 buffer and treated with Benzonase (Merck KgA, Darmstadt, Germany) at a final concentration of 150 U/mL at 37°C for 1 h.

3.1.2. Chromatography media

Merck (Darmstadt, Germany) provided the chromatographic resins used in this work. Due to proprietary reasons, resins are here referred as resin A and resin B. Resin A backbone consists of synthetic methacrylate polymer beads while resin B backbone consists of rigid hydrophilic polyvinyl ether polymer beads. Both resins are functionalized with “tentacles”, long linear polymer chains that carry the functional ligands. In both cases, the functional group is the quaternary ammonium ion trimethylammoniumethyl (TMAE or Q). Thus, both resins are strong anion exchangers. According to the manufacturer specifications, resin A has a particle size in the range of 40-90 µm in diameter and a pore size of about 80 nm in diameter. Resin B has a mean particle size of 50 µm in diameter.

3.2 Methods

3.2.1. Resin structure and physicochemical properties

The particle size distribution of each resin was determined from micrographs taken with a light microscope at 10x or 40x magnification. Both resins were washed and equilibrated in 50 mm HEPES, pH 7.2 buffer before visualized at the microscope. For each resin, several micrographs were taken in order to collect images of at least 500 particles. The software Image J (available at https://imagej.nih.gov/ij/) was used to measure the diameter of single circular particles by converting a scale of known distance into pixels. Moreover, from the particle size distribution, the volume-average diameter was calculated.

Transmission electron microscopy (TEM) was used to observe the internal structure of virgin and saturated resins. In both cases, previously to the TEM sample preparation, resins were washed and equilibrated with binding buffer (50 mM HEPES, pH 7.2). Saturated resins were prepared by incubating the resin particles with protein (bovine serum albumin, BSA) or VLP (HIV-1 gag VLP) in binding buffer, during 24h at room temperature. After the incubation with protein/VLP, resins were washed with binding buffer and chemically fixed with 2% Glutaraldehyde for 20 min at room temperature. For the preparation of the specimens for TEM, all resin samples (virgin, BSA-saturated and VLP-saturated) were dehydrated with increasing ethanol concentrations from 0 to 100% anhydrous ethanol, embedded in LRWhite resin (London Resin Company, Ltd., London, UK) and ultramicrotomed into 80 nm sections as previously described in [37]. The sections were then stained with lead citrate followed by uranyl acetate and imaged with a JEOL 1230 instrument (JEOL, Tokyo, Japan) [38].

The density of the hydrated resin was measured using a pycnometer. To obtain the hydrated resin, small aliquots (~500 µL) of resin slurry (50% v/v settled resin in 50 mM HEPES, pH 7.2) were centrifuged, using micro-centrifuge filter tubes, in order to remove the extraparticle fluid. To optimize the centrifugation conditions, samples were centrifuged at various sequential speeds (2500, 5000, 7500, 10000 rpm) during 15 min until no significant change in the sample mass was observed. Additionally, a calibration curve was constructed for accessing the mass of hydrated resin in a certain volume of settled resin in a 50% slurry (50 mM HEPES, pH 7.2). For this purpose, aliquots of different volumes were centrifuged at 10000 rpm during 20 min using micro-centrifuge filter tubes and the mass of the hydrated resin measured using a laboratory scale.

3.2.2. Column packing, mechanical and flow properties

Resins A and B were packed into Tricorn 0.5 x 15 cm columns following the manufacturer's instructions. Prior to the packing, resins were washed, equilibrated with pre-packing buffer (Resin A: 50 mM HEPES, 300 mM NaCl, pH 7.2; resin B: 50 mM HEPES, 2000 mM NaCl, pH 7.2) and let settle down in a volumetric cylinder overnight. Both resins slurries were adjusted to 50% (v/v). Resin A was flow-packed, using 50 mM HEPES, 150 mM NaCl, pH 7.2 buffer, with an ÄKTA Pure system at constant flow rate (2.5 mL/min, ~760 cm/h). Resin B was vacuum-packed, using 50 mM HEPES, 150 mM NaCl, pH 7.2 buffer. Increasing flow rates (0.5, 1.25, 2.5, and 3.75 mL/min) were applied during column B packing.

The quality of the packing was determined by calculating the reduced HETP (h) and peak asymmetry factor (A_s) of a pulse injection of NaCl into each column. Both resins were tested at a linear flow rate of 100 cm/h, using 100 µL of 1 M NaCl as sample. The mobile phase for resin A was 200 mM NaCl and for resin B 150 mM NaCl.

The flow properties of the columns were evaluated by determining the pressure drop (ΔP) using increasing linear flow rates of 50, 100, 200, 300 and 400 cm/h for resin A and 100, 250, 500, 750 and 1000 cm/h for resin B.

3.2.3. Inverse size exclusion chromatography

Inverse size exclusion chromatography (iSEC) was used to determine the accessible intraparticle porosity and apparent pore radius distribution of each resin. For this purpose, the isocratic retention volumes of several standards with different molecular weights were determined using an Alliance e2695 HPLC system (Waters Corporation, Milford, MA, USA) with a refractive index detector. The retention volume of each standard was corrected accounting for the extra-column volume, which was determined by injecting the smallest and biggest standards into an empty column (top and bottom adaptors were closed against each other). Before the injections of the standards, columns were equilibrated with working buffer. Different salt concentrations (0.1, 1 and 2 M NaCl in 50 mM HEPES, pH7.2 buffer) were used. For each column, a series of 20 µL injections of 5 mg/mL glucose and dextran standards were made and eluted at 0.5 mL/min flow rate. The hydrodynamic radii (r_s) of each standard was estimated using the correlation of Hagel et al [39], where M_s is the molecular weight of the standard:

$$r_s = 0.0271 \times M_s^{0.498}$$

Table 3.1. Inverse size exclusion chromatography (iSEC) standards' hydrodynamic radius (r_s).

Standard	r_s (nm)
Glucose	0.4
Dextran 4 kDa	1.7
Dextran 10 kDa	2.7
Dextran 40 kDa	5.3
Dextran 70 kDa	7.0
Dextran 80 kDa	7.5
Dextran 150 kDa	10.2
Dextran 270 kDa	13.7
Dextran 2000 kDa	37.2

3.2.4. Batch uptake (VLP adsorption kinetics)

The kinetics of VLP adsorption and desorption were determined by batch uptake measurements as described by Carta et al [40]. For the adsorption experiments, resin beads (previously equilibrated in binding buffer, 50 mM HEPES, pH 7.2) were suspended in an agitated vessel containing a VLP solution (in binding buffer). The solution was continuously recirculated through a UV (A280 nm) spectrometer using a peristaltic pump. A 5 µm membrane filter was used to prevent the resin particles from entering the UV detector. Figure 7 shows a schematic representation of the batch apparatus and sample data. VLP solution concentration and resin amount were adjusted in order to achieve a 50% change in the VLP concentration during the experiment. Calculations were made based on the maximum binding capacity for each resin obtained by the respective adsorption isotherms. The initial and final VLP concentration was accessed by off-line measurements of the UV absorbance at 280 nm. A mass balance was used to determine the amount of VLP adsorbed to the resin at each time point of the experiment.

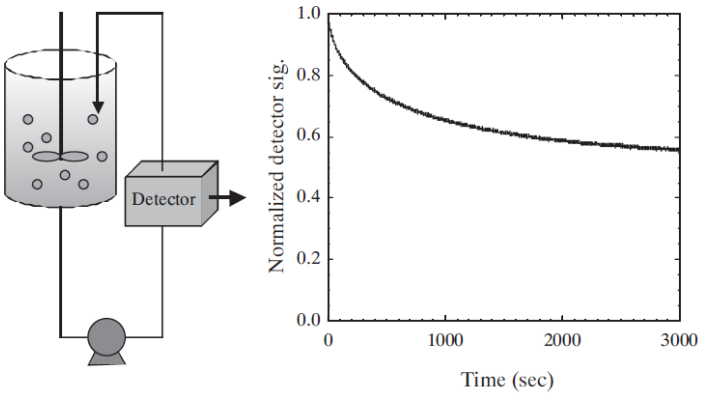

Figure 7. Schematic representation of a stirred batch apparatus and sample data (from [40]).

3.2.5. Confocal laser scanning microscopy

In confocal laser scanning microscopy (CLSM), the localization and concentration of a fluorophore present in a three-dimensional transparent matrix is obtained by collecting the emitted fluorescence in a thin optical section.

Enveloped VLPs were labelled using PKH26 Red Fluorescent Cell Linker kit (Sigma-Aldrich, St. Louis, MO, USA) according to the manufacturer instructions. The labelling occurs by the partitioning of the lipophilic dye into the VLP envelope (Figure 8-A). Since there are no limiting binding sites for the dye on the VLP surface, and in order to maintain the VLP integrity, we used a concentration of dye that results in about 10% VLP surface coverage (assuming that the PKH26 molecule has a circular footprint of about 1.3 nm in diameter, Figure 8-B).

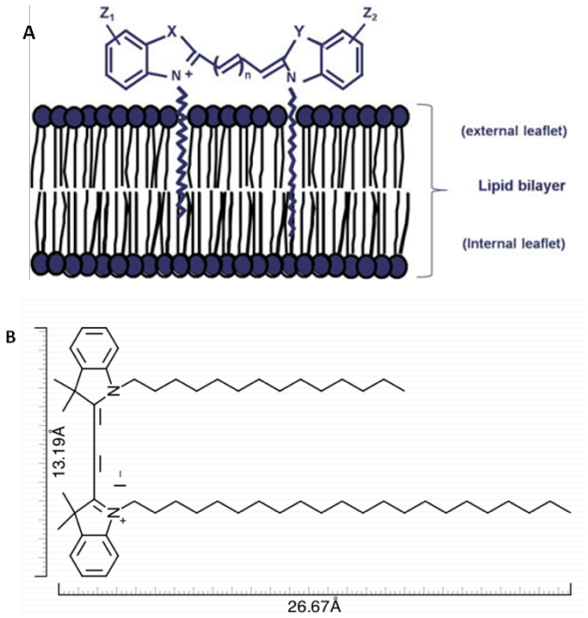

Figure 8. (A) Schematic representation of the partitioning of PKH dyes into the cell membrane; (B) Chemical structure of the PKH26 dye (*Patent WO1998033530 A1*).

Immediately after the labelling reaction, the mixture was injected into a desalting column (HiPrep 20/10, GE Healthcare, Piscataway, NJ, USA) in order to remove possible free dye molecules and buffer exchange the labelled VLPs into 50 mM HEPES, pH 7.2 buffer.

CLSM was used to observe the adsorbed fluorescently labelled VLPs within individual resin beads. For this purpose, resin beads, pre-equilibrated in binding buffer, were incubated with a VLP solution containing 1:1 ratio of labelled to unlabelled VLPs, with a final concentration of about $2x10^{11}$ particles/mL. In order to maintain excess of VLP during the adsorption experiments, the resin amounts were adjusted considering the maximum binding capacity of each resin, so that the change in the VLP concentration was less than 10%. To access the adsorption kinetics using CLSM, small samples containing resin beads with adsorbed VLPs (100 µL) were taken from the incubation slurry at different time points. The extraparticle solution was removed by centrifuging the sample in a microfilter

centrifuge tube at 10000 rpm for 30 seconds. The beads were then re-suspended in 40 µL of 50% (w/v) sucrose solution and placed on a microscope slice. A Zeiss LSM 510 microscope with a 40x1.3 (oil) objective (Carl Zeiss MicroImaging, LLC, Thornwood, NY) was used to image the resin beads at an excitation wavelength of 561 nm and an emission wavelength greater than 575 nm. All images were taken at the equator of the beads. The microscope settings (e.g. laser intensity, pinhole, detector gain) were defined using VLP-saturated beads (24h incubation) and kept equal for the entire set of samples.

4 Results and Discussion

4.1 Polymer grafted chromatography media properties

The particle size distribution of both resins was obtained from micrographs taken with a light microscope (Figure 9). Despite the manufacturer's statement of a particle size in the range of 40-90 µm for resin A, we found a larger particle size distribution, in the range of 50-110 µm, with a volume-averaged particle diameter of 82 µm. Resin B was found to have a narrower particle size distribution, in the rage 35-70 µm, and a volume-averaged particle diameter of 49 µm, which is in accordance with the value of 50 µm claimed by the manufacturer.

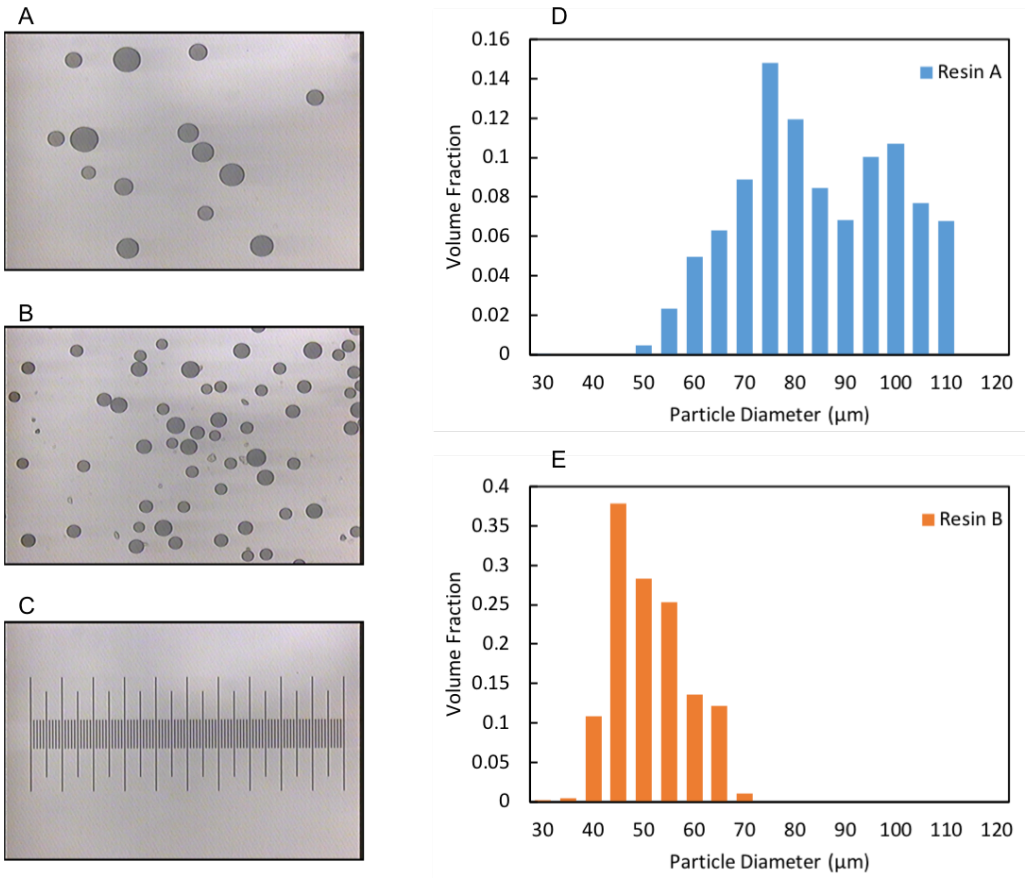

Figure 9. (A) Light microscope micrograph of resin A; (A) Light microscope micrograph of resin B; (C) Microscopic ruler; (D) Particle size distribution of resin A; (E) Particle size distribution of resin B.

The internal structure of both resins was observed using transmission electron microscopy. Figure 10 shows the transmission electron micrographs taken near the bead surface (marked with the arrow) of virgin, VLP-saturated and BSA-saturated resin A and virgin and VLP-saturated resin B.

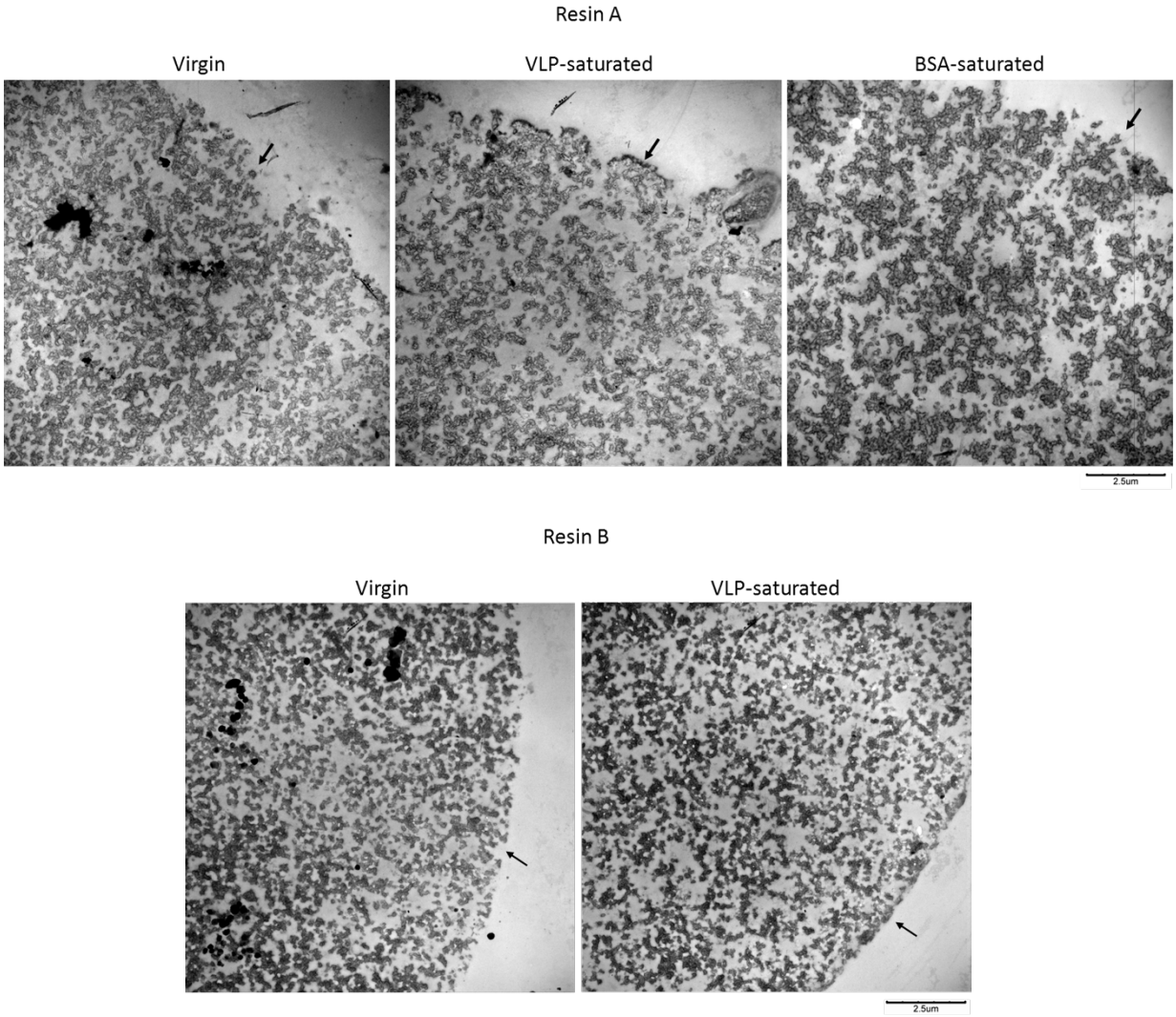

Figure 10. Transmission electron micrographs of virgin, VLP-saturated and BSA-saturated resin A and virgin and VLP-saturated resin B at 5000x magnification.

The uniform light grey area (outside and inside the bead) is the LRWhite embedding matrix which fills the empty spaces. The medium-dark grey areas present in all images correspond to the resin backbone. The BSA-saturated resin A shows dark-grey, heavily stained areas on the resin backbone across the entire bead, which correspond to the bound BSA. On the other hand, the VLP-saturated resin A only shows these dark-grey stained areas on the outer surface of the bead. These images

clearly show that the VLP adsorption occurs exclusively on the outer surface of the beads. The same VLP adsorption behaviour can be observed for resin B.

A pycnometer was used to determine the densities of the hydrated resins (equilibrated in working buffer, 50 mM HEPES, pH 7.2). Values of 1.09 and 1.08 g/mL were determined for resin A and B respectively.

To determine the optimum centrifugation conditions for removal of extraparticle liquid from a resin slurry sample, a microfilter centrifuge tube was used and several centrifugation speeds were tested. Figure 11 shows the reduction on the hydrated resin residual mass after each sequential centrifugation step. For both resins, to ensure the removal of the extraparticle liquid, the selected centrifugation conditions were 10000 rpm and 20 minutes.

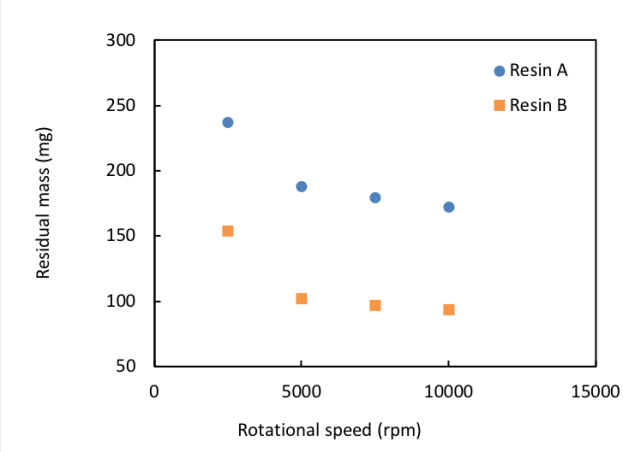

Figure 11. Residual hydrated resin mass after sequential centrifugation steps of a resin slurry sample in a microfilter centrifuge tube.

Since different experiments require different resin preparations, such as hydrated resin to be weighed or resin slurry to be pipetted or packed in a column, the mass of hydrated resin in certain volume of settled resin, in a 50% (v/v) slurry, was determined (Figure 12). For both resins, a sample with 100 µL of settled resin contain about 64 mg of hydrated resin.

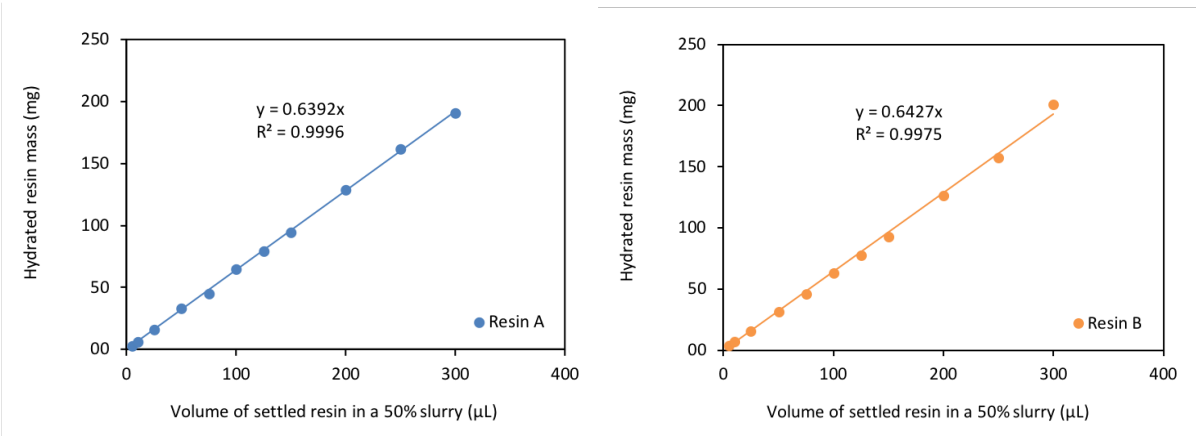

Figure 12. Relation between the resins settled bed volume in a 50% (v/v) slurry and the hydrated resin mass.

4.2 Column packing, mechanical and flow properties

Resin A and B were packed into Tricorn columns following the manufacturer's instructions. Column A (packed with resin A) had a final bed height of 14.5 cm, resulting in 2.85 mL of packed bed and column B (packed with resin B) a height of 14 cm, with a corresponding 2.75 mL packed bed. In both cases, the packing quality was determined by calculating the reduced HETP (h) and the asymmetry factor (A_s) of a NaCl pulse injection into the column (Figure 14). Figure 13 shows how reduced HETP and asymmetry factor can be calculated based on the elution peak of an inert tracer. Reduced HETPs in the range of 2-10 and asymmetry factors in the range of 0.8-1.2 are typical for a well-packed column and indicate a reasonably homogeneous flow [31]. Table 4.1 summarizes the reduced HETP and asymmetry values determined for each one of the columns. Since all values are within the accepted ranges, both columns can be considered as well packed.

Table 4.1. Properties of the packed columns determined by the pulse injection of NaCl.

	Column A	**Column B**
Asymmetry, A_s	0.97	1.12
Reduced HETP, h [Moment method]	7.55	9.43
Reduced HETP, h [Graphical method]	7.60	9.59

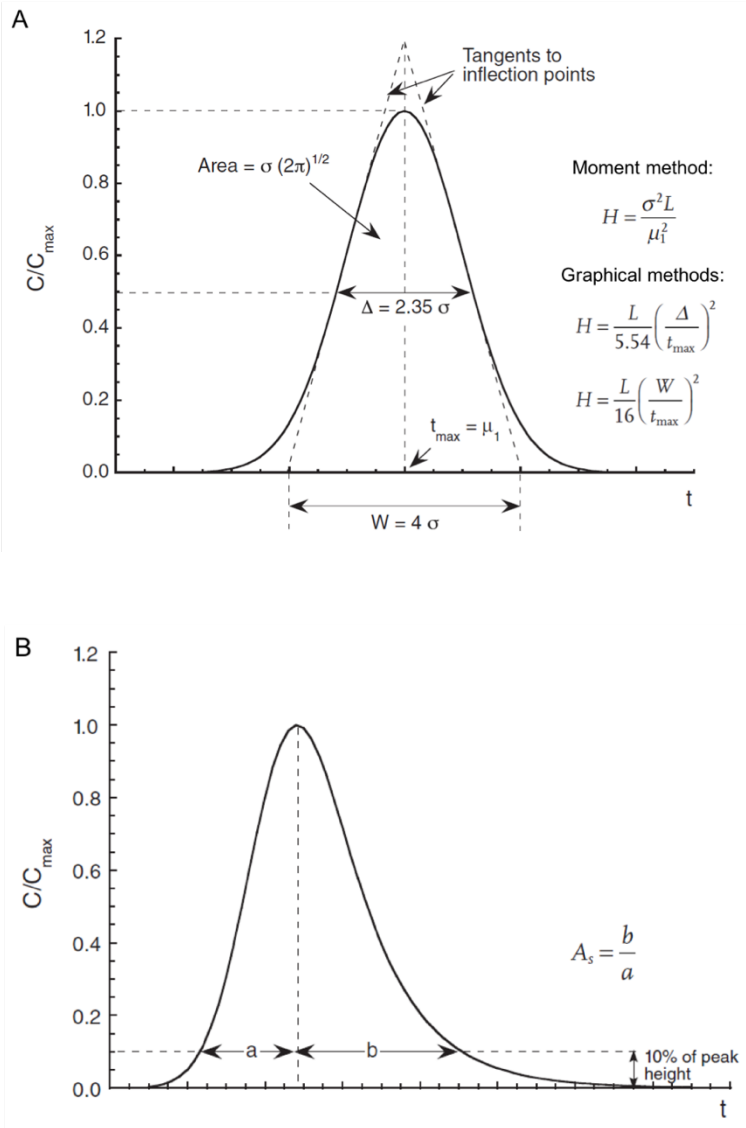

Figure 13. (A) Parameters used for the calculation of HEPT (H). In the "moment method", μ_1 is the peak first moment or mean elution time and σ^2 is the peak second moment or peak variance. This method can be used for both symmetrical and asymmetrical peaks. The graphical method is based on the properties of a Gaussian peak, thus it can only be used for symmetrical or nearly symmetrical peaks; The reduced HETP (h) is obtained dividing the HETP by the particle diameter. (B) Parameters used for the calculation of the peak asymmetry factor (adapted from [31]).

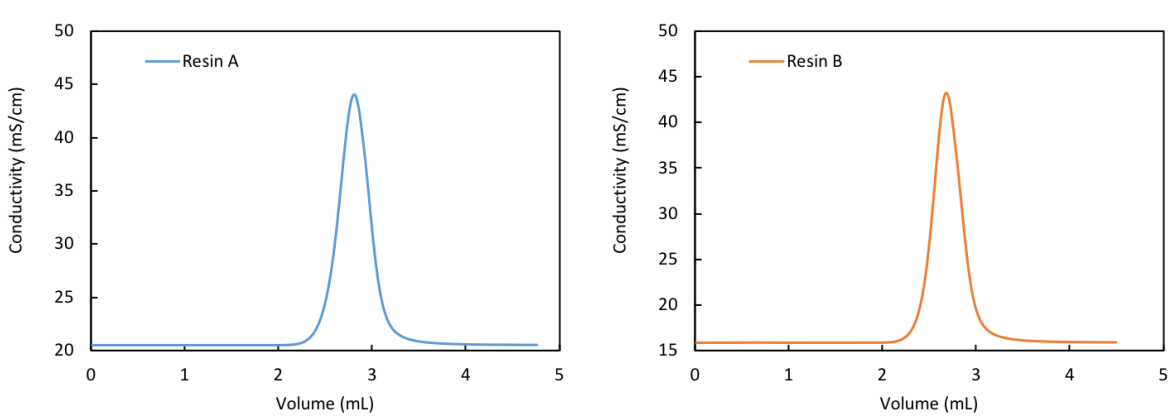

Figure 14. Isocratic elution peaks of NaCl injections in column A (resin A) and column B (resin B).

Additionally, since NaCl is a small molecule, able to enter the resin pores, it is possible to calculate the column total porosity (ε_T) from the NaCl elution peaks using the following equation:

$$\varepsilon_T = \frac{\mu_{NaCl} - \mu_{extra}}{V_{column}}$$

where, μ_{NaCl} is the first moment or elution volume of the NaCl peak, μ_{extra} is the extra column volume and V_{column} is the column volume. Values of 0.88 and 0.87 were obtained for the total porosity (ε_T) of resin A and resin B respectively.

The pressure drop (ΔP) was determined for both columns using sequential increasing flow rates. The pressure flow behaviour of a column is determined by the mechanical properties of the resin particles and their size. When using incompressible particles, the flow in a packed column follows Darcy's law:

$$\Delta P = \frac{\eta u L}{B_0}$$

where η is the mobile phase viscosity, u is the superficial velocity, L is the column length and B_0 is the hydraulic permeability. The latter depends on the particle size and packing density and, for rigid particles, can be estimated using the Karman-Cozeny equation:

$$B_0 = \frac{d_p^2 \varepsilon^2}{150(1-\varepsilon)^2}$$

where d_p is the particle diameter and ε the extraparticle porosity. Combining these two equations it is possible to estimate the extraparticle porosity only by measuring the column pressure drop [31].

Figure 15 shows the pressure-flow profiles for both columns and table 4.2 summarizes the calculated parameters. The hydraulic permeability was calculated from the slope of the linear regression using Darcy's law and the extraparticle porosity was estimated using the Karman-Cozeny equation.

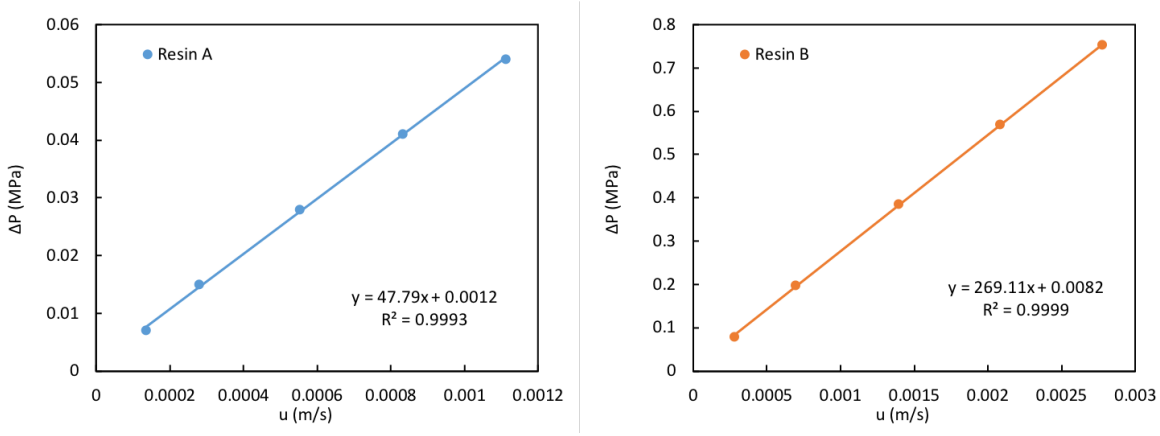

Figure 15. Pressure-flow profiles of column A and B. Equation were obtained from a linear regression fitting of the experimental data.

Table 4.2. Hydraulic permeability (B_0) and extraparticle porosity (ε) calculated from pressure drop (ΔP).

	Column A	**Column B**
Hydraulic permeability, B_0 (m^2)	3.0×10^{-12}	5.2×10^{-13}
Extraparticle porosity, ε	0.32	0.26

As expected due to the smaller particle size, resin B presents a smaller hydraulic permeability and consequently higher pressures are observed when comparing to resin A at the same superficial velocity. It should be mentioned that despite resin A particles are compressible, the experiments were performed at smaller superficial velocities than the packing velocity, avoiding the compression of the packed bed.

4.3 Inverse size exclusion chromatography

Inverse size exclusion chromatography (iSEC) was used to determine the intraparticle porosity (ε_p), the pore size distribution and the pore radii (r_p). Figure 16 shows an example of iSEC chromatograms from resin A when using 50 mM HEPES, 2 M NaCl, pH 7.2 as mobile phase. Results show that the high molecular weight standards elute earlier than the low molecular weight ones. Since small molecules are able to enter the resin pores, they have access to a larger fraction of the particle volume, requiring higher volumes to elute. On the other hand, big molecules that are excluded from the resin pores, travel exclusively along the extraparticle volume of the column, requiring smaller volumes to elute. Similar results were obtained for resin B and for all the tested salt concentrations.

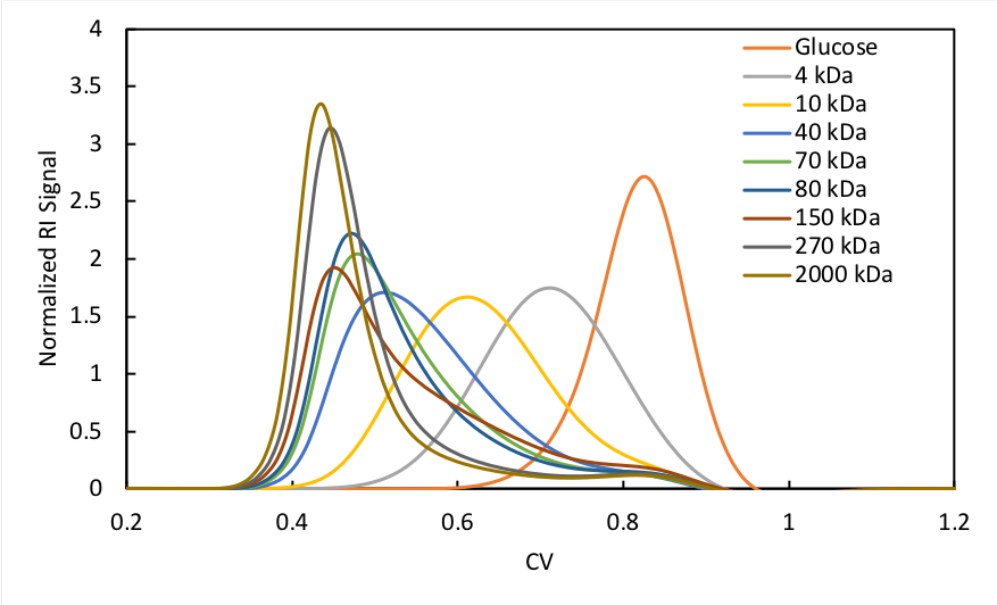

Figure 16. Chromatograms from iSEC of resin A when using 50 mM HEPES, 2 M NaCl, pH 7.2 as mobile phase. Reflective index (RI) signal was normalized by the peak area.

From each one of the chromatograms, the peak retention volume (V_R) was used to calculate the distribution coefficient (K_D) using the following equation:

$$K_D = \frac{V_R/V_{column} - \varepsilon}{(1-\varepsilon)}$$

where, V_{column} is the column volume and ε the extraparticle porosity, which can be determined from the retention volume of a molecule that is completely excluded from the pores, such as the 2000 kDa Dextran standard, using the following equation:

$$\varepsilon = \frac{V_{2000\ kDa\ Dextran} - \mu_{extra}}{V_{column}}$$

The distribution coefficient (K_D) can be related to the resin pore size using a simple model which considers the partitioning of spherical molecules (with r_m radius) in cylindrical pores as represented in Figure 17. Thus, K_D can be calculated using the following equation:

$$K_D = \varepsilon_p \left(1 - \frac{r_m}{r_{pore}}\right)^2$$

where, r_m is the radius of the standard molecule and r_{pore} the radius of the resin pores. This simplistic model can be used to easily determine mono- or bi-modal pore size distributions. However, in some cases, resin pores can be extremely heterogeneous and have wide-ranging pore size distributions, requiring a more complex model to fit the experimental data.

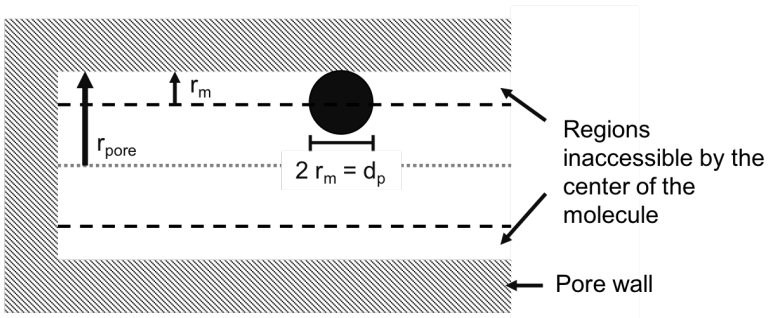

Figure 17. Partitioning of a spherical solute in a cylindrical pore (adapted from [31]).

A log normal distribution function can be used to describe the pore size distribution in a more realistic way using the following equation [41]:

$$f(r) = \frac{1}{r} exp\left[-\frac{1}{2}\left(\frac{log(r/r_p)}{s_p}\right)^2\right]$$

where the parameters r_p and s_p measure the mode and the width of the distribution respectively. Considering the same partitioning model (spherical molecule in a cylindrical pore, Figure 17) and that the fractional accessible volume is described by $[1-(r_m/r)]^2$, K_D can then be calculated for a given standard from the ratio between accessible pore volume and total pore volume by [41]:

$$K_D = \frac{\int_{r_m}^{\infty} f(r)[1-(r_m/r)]^2 dr}{\int_0^{\infty} f(r)dr}$$

Figure 18 shows the determined distribution coefficients for the different standards. Dots represent K_D values calculated from experimentally measured retention volumes. Curves represent the log normal cylindrical pore model (f(r)), which distribution parameters, r_p and s_p, were calculated by least-squares fitting of experimental K_D values. Figure 19 shows the estimated pore size distribution for each one of the resins and conditions and Table 4.3 the respective distribution parameters. Physically, a K_D value of zero refers to a molecule that is completed excluded from the pores and a K_D value of one refers to a molecule that is completely included in the pores. Consequently, larger standards have smaller K_D values and vice-versa.

Figure 19 and Table 4.3 additionally show that the increase in the ionic strength of the mobile phase from 0.1 to 1 M NaCl resulted wider pore size distributions, higher s_p values, and increased pore radius, higher r_p values. This can be explained by the chemical properties of the polymer chains ("tentacles") grafted on the resin's surface. At low salt concentrations, the charged tentacles have an extended three-dimensional arrangement which derives from the electrostatic repulsion within and between polymer chains. However, as ionic strength increases (by increasing the salt concentration), the screening of the charges in the polymer chains supresses the repulsion interactions leading to the collapse and compaction of the tentacles. This change in the tentacles' three-dimensional arrangement gives origin to larger pores with increased accessibility [41]. Still, the further increase in the ionic strength of the mobile phase from 1 to 2 M NaCl showed little or no increase in the pore radius and/or accessibility. This suggests that the maximum compaction of the tentacles already occurred with 1 M NaCl on the mobile phase (lower salt concentrations can be tested to find the minimum ionic strength necessary to reach the maximum pore accessibility).

Regarding the distribution coefficient, in Figure 18 it can be observed that when using higher salt concentrations in the mobile phase (from 0.1 to 1 or 2 M NaCl) the K_D value for intermediate size standards is higher. Once more, this is related to the larger pore accessibility caused by the tentacles compaction. However, for the smaller and bigger standards no change in the K_D values was observed. For the smaller standards this can be explained because they have full access to the total porosity even if the tentacles are extended and fill most of the pore volume. On the other hand, the bigger standards are completely excluded from the pores even when the tentacles collapsed and the pores are wider.

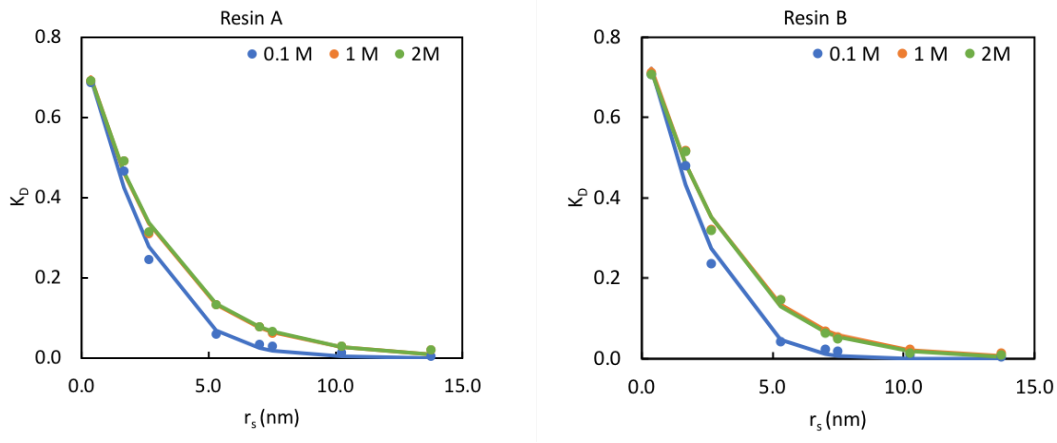

Figure 18. ISEC calibration curves for resin A and resin B at different salt concentrations (0.1, 1 and 2 M NaCl). Dots: K_D calculated from the experimentally measured retention volumes; Lines: K_D calculated from the log normal cylindrical pore model.

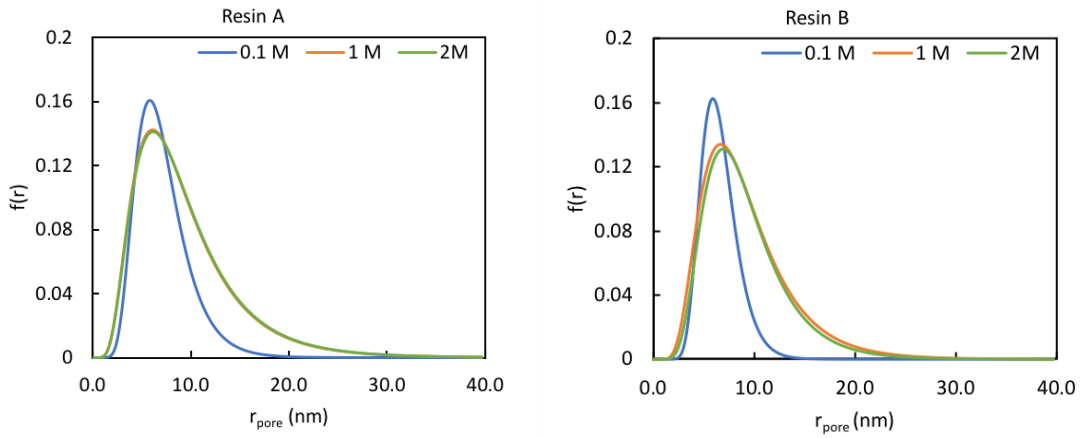

Figure 19. Estimated pore size distribution for resin A and resin B at different salt concentrations (0.1, 1 and 2 M NaCl).

Table 4.3. Dimension parameters calculated from the log normal cylindrical pore model.

	Resin A			**Resin B**		
NaCl (M)	**0.1**	**1**	**2**	**0.1**	**1**	**2**
ε	0.42	0.43	0.43	0.37	0.38	0.38
ε_p	0.79	0.78	0.78	0.81	0.80	0.79
$\varepsilon_T = \varepsilon + (1-\varepsilon)\varepsilon_p$	0.88	0.88	0.88	0.88	0.88	0.87
r_p (nm)	6.66	8.10	8.18	6.38	8.29	8.33
s_p (nm)	0.37	0.53	0.53	0.27	0.46	0.42

The total porosity, ε_T, in Table 4.3 was calculated using the intra- and extraparticle porosities (ε_p and ε) determined in the iSEC experiment. The obtained values are in accordance with the values obtained from the NaCl pulse injections for both resins. The deviations observed for the extraparticle porosity calculated using pressure drop experiments and the iSEC experiments can be explained because of the flow fluctuations in the ÄKTA system and also the accuracy of the pressure sensors. Additionally, it is known that due to their geometry, the densest packed spheres use approximately 74% of the volume and random packed spheres generally have a density around 64%. Thus, for a chromatographic packed bed, the minimum extraparticle porosity should be 0.26 and the expected values should be around 0.36. Since from the pressure drop experiments the determined extraparticle porosities were 0.32 and 0.26 for resin A and resin B respectively and these values are lower than expected, for any further calculations the intra-, extra- and total porosity values from Table 4.3 were used.

4.4 Batch uptake (VLP adsorption kinetics)

Batch uptake experiments were used to access the adsorption kinetics as described by Carta et al [40]. Since VLPs are not able to enter the resin pores and bind only on a thin shell in the outer surface of the resin beads, external mass transfer is an important resistance in the overall mass transfer phenomenon. The flow conditions of the system were estimated using engineering correlations for impellers in agitated systems. Reynold's number for the impeller (Re_i) was determined by:

$$Re_i = \frac{N d_i^2 \rho}{\mu}$$

where, N is the impeller angular velocity, d_i the impeller diameter, ρ the solution density and μ the dynamic viscosity. The obtained value (Re_i = 2970) specifies a turbulent regime for the used batch system. From a plot of power number versus Reynold's number and geometry of impeller, the power number was found to be 2. The power consumption per unit of fluid (ε) was then calculated using the following equations:

$$\bar{\varepsilon} = \frac{P}{V\rho}$$

$$P = N_P N^3 d_i^5 \rho$$

where, P is the power consumption, V the solution volume and N_p the power number. These parameters were used to calculate the resin particle Reynold's number (Re_p) using the following equation:

$$Re_p = \left(\frac{\bar{\varepsilon} d_p^4}{\upsilon^3}\right)^{1/3}$$

where, d_p is the diameter of the particle and υ the kinematic viscosity. Additionally, Schmidt (Sc) and Sherwood (Sh) numbers were calculated by:

$$Sc = \frac{\upsilon}{D_0}$$

$$Sh = 2 + 0.52 Re_p^{0.52} Sc^{1/3}$$

where, D_0 is the molecular diffusion rate. Finally, the external mass transfer coefficient, k_f, was calculated by:

$$k_f = \frac{Sh D_0}{d_p}$$

where, d_p is the resin particle diameter. Table 4.4 summarizes the calculated values for the referred parameters.

Table 4.4. Mass transfer parameters obtained using engineering correlations.

	VLPs	
D_0 (cm^2/s)	3.27×10^{-8}	
Sc	2.72×10^{5}	
	Resin A	**Resin B**
Re_p	1.74	0.88
Sh	46.95	33.46
k_f (cm/s)	1.87×10^{-4}	2.23×10^{-4}

Previous experiments performed with the same batch uptake system revealed that external mass transfer coefficient estimated using engineering correlations is in accordance with the directly measured one using the method proposed by Armenante and Kirwan (1989).

Figure 20 shows examples of batch uptake experiments. For both resins, immediately after the addition of the resin to the VLP solution, a fast decrease in VLP concentration can be observed. This decrease in concentration is directly related to the adsorption of the VLPs on the chromatography resin. For both resins, two phases of adsorption can be observed. For resin A, the initial fast rate of adsorption decreases after about 15 minutes. Nevertheless, adsorption can still be observed up to 3 hours. Resins B shows a fast adsorption rate up to about 8 minutes, followed by a slower adsorption rate up to 3 hours. In the end of each experiment, at equilibrium, the maximum binding capacity of each resin was reached.

The modelling of the experimental data was done using a batch uptake model for rectangular isotherms based on the two-film model of Yoshida and Ruthven (1984) and assuming that adsorption occurs in a shell. This model, developed by Giorgio Carta (2018), considers the adsorption with a rectangular isotherm restricted to a thin layer at the particle surface between the radial position r_s and r_p as represented in Figure 21.

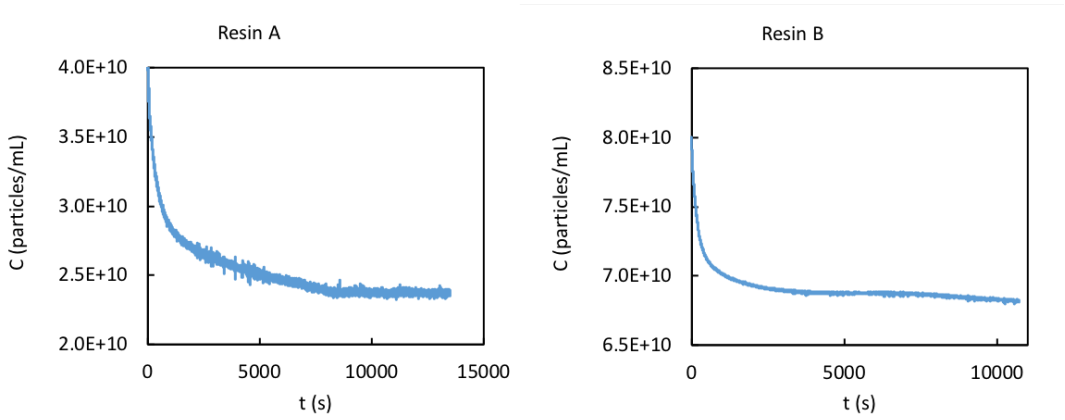

Figure 20. Batch uptake profiles for VLP adsorption using resin A and resin B. The VLP concentration (C) is plotted against the time (t).

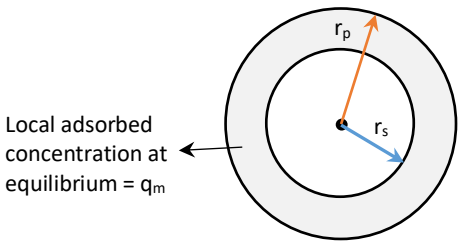

Figure 21. Adsorption on a thin shell at the particle surface between the radial position r_s and r_p (particle radius).

The volume of the adsorbing shell (V_s) can be calculated by:

$$V_s = \left[1 - \left(r_s/r_p\right)^3\right] V_p$$

where, V_p is the resin particle volume. The adsorbed concentration averaged over the total particle volume (q_p) is described by:

$$q_p = \left[1 - \left(r_s/r_p\right)^3\right] q$$

or, at equilibrium by:

$$q_{m,p} = \left[1 - \left(r_s/r_p\right)^3\right] q_m$$

where, $q_{m,p}$ and q_m are the adsorbed concentrations averaged over the total particle volume and in the thin shell respectively, both at equilibrium.

Following the model proposed by Yoshida and Ruthven (1984), the rate of adsorption (dq/dt) is described by two film resistances in series:

$$\frac{dt}{dq} = k_c(C_0 - C) = k_q(q_s - q)$$

where, q is the adsorbed concentration averaged over the adsorbed layer, k_c is the external rate coefficient, C is the bulk solution concentration, k_q is the internal rate coefficient and q_s the actual adsorbed concentration at the particle surface. The overall material balance is given by:

$$V_s \frac{dq}{dt} = -V \frac{dC}{dt}$$

$$V_s q = V(C_0 - C)$$

The external rate coefficient (k_c) is related to the boundary mass transfer coefficient (k_f) according to:

$$k_c = \frac{3k_f}{r_p\left[1 - \left(r_s/r_p\right)^3\right]}$$

The internal rate coefficient k_p is an empirical parameter.

Following Yoshida and Ruthven (1984), the batch uptake process is divided in two steps. In the first step (t < t'), the solution concentration at the particle surface (C_s) is zero and the overall process is controlled by the external rate coefficient. Accordingly, the adsorption can be described by:

$$\frac{dq}{dt} = k_c C$$

$$-\frac{V}{V_s}\frac{dC}{dt} = k_c C$$

Integrating this equation gives:

$$C = C_0\, exp\left(-\frac{k_c V_s}{V} t\right)$$

During this step, the adsorbed concentration is given by:

$$q_s = q + \frac{k_c}{k_q} C$$

This first step ends when $q_s = q_m$. Thus, t' can be found as:

$$q_m = \frac{V C_0}{V_s}\left[1 - exp\left(-\frac{V_s k_c}{V} t'\right)\right] + \frac{k_c C_0}{k_q} exp\left(-\frac{V_s k_c}{V} t'\right)$$

or:

$$t' = -\frac{V}{V_s k_c} ln\left(\frac{q_m - \frac{V C_0}{V_s}}{\frac{k_c C_0}{k_q} - \frac{V C_0}{V_s}}\right)$$

and:

$$q' = \frac{V C_0}{V_s}\left[1 - exp\left(-\frac{k_c V_s}{V} t'\right)\right]$$

During the second step (t > t'; $q_s = q_m$), the overall process is controlled by the internal rate coefficient. Thus, the adsorption is described by:

$$\frac{dq}{dt} = k_q (q_m - q)$$

Integrating this equation, the adsorbed concentration is given by:

$$q = q_m - (q_m - q')\, exp\left[-k_q(t - t')\right]$$

and:

$$C = C_0 - \frac{V_s}{V} q$$

Valid for C > 0.

Figure 22 shows the experimental and modelled VLP adsorbed concentration averaged over the total particle volume (q_p) for resin A and resin B. In both cases it is possible to observe that the model does not fully describe the experimental behavior. For resin A, the adsorption is faster than predicted by the model. For resin B, despite the initial adsorption is well predicted by the model, the transition phase is slower than the model predicts. From our knowledge the UV detection is not the most accurate for VLPs. Batch uptake experiments will be repeated using other detection methods such as Multi-angle Light Scattering (MALS) and/or Nanoparticle Tracking Analysis (NTA) [These techniques were not available during my stay abroad]. Furthermore, additional models will be developed in order to account for possible multilayer formation and binding resistances.

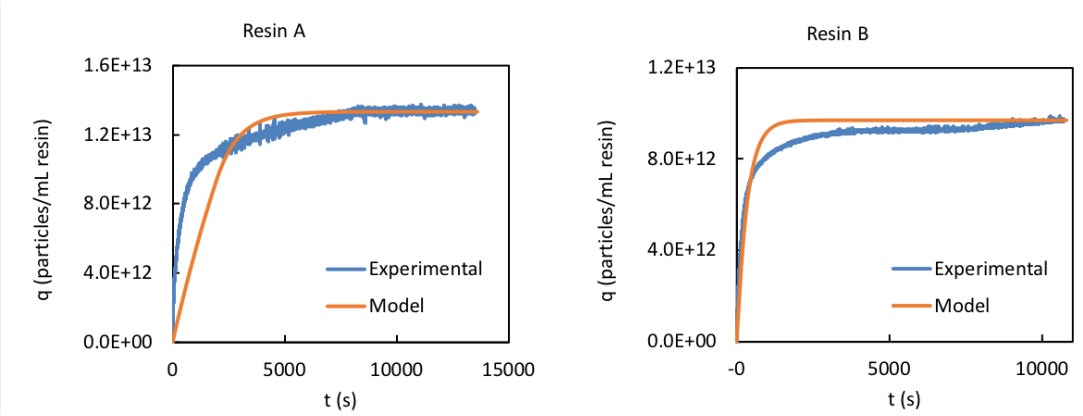

Figure 22. Batch uptake VLP adsorbed concentration averaged over the total particle volume (q_p).

4.5 Confocal laser scanning microscopy

Confocal Laser Scanning Microscopy (CLSM) was used to observe the adsorbed fluorescently labelled VLPs within individual resin beads. Figure 23 shows confocal micrographs of cross sections of resin A with adsorbed fluorescently labelled VLPs at different incubation times. Again, as expected, the VLP adsorption exclusively occurs in the outer surface of the resin beads. The adsorption is fast and after only 5 minutes of incubation a full ring around the resin bead can be observed. Despite no penetration of the fluorescent labelled VLPs into the resin beads is observed, it is possible to notice an increase in the fluorescence intensity of the adsorption ring over time. These results are in accordance with the initial fast VLP adsorption followed by slower uptake observed in the batch experiments. Resin B showed the same behaviour (data not shown).

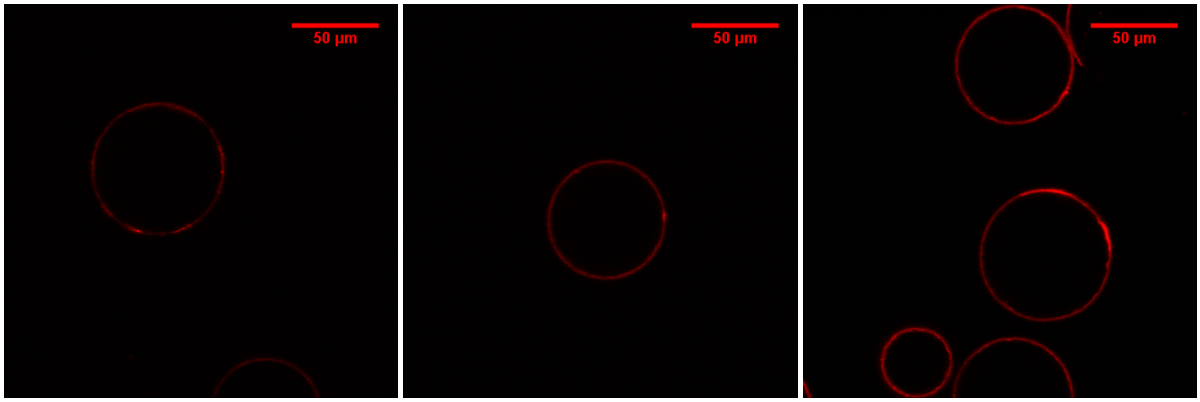

Figure 23. Transient profiles of VLP adsorption in resin A at different incubation times. Left: 5 minutes; middle: 1 hour; Right: 24 hours. Laser intensity settings were kept constant after set using the 24h sample to avoid over-exposure.

5 Conclusion

Through this study, the adsorption and transport mechanisms of VLPs onto polymer grafted chromatography media were investigated. Two different anion exchangers were used. Both resins contain the same ligand chemistry but different backbones, particle sizes and particle pore sizes. Nevertheless, in both cases the mechanisms were similar.

One of the main findings of this work is that the VLPs bind exclusively on the outer surface of the resin beads. Both resins have small pore diameters (shown by the iSEC data) when compared to the VLP diameter, suggesting that the VLPs are not able to enter the pores. The binding of the VLPs exclusively at the outer surface of the resin beads was confirmed by both TEM and CLSM micrographs. Therefore, the available surface area is one of the most important parameters for the VLP binding capacity in this type resins. Consequently, when modelling the adsorption mechanisms, the particle size distribution should be considered, especially for resin A which has a very wide distribution. Moreover, TEM micrographs showed that the resin beads are not perfect spheres, having some “open pore areas” at their surface and consequently the surface area might be higher than the surface area of a sphere with the same diameter. This fact can justify increased binding capacities even though only binding at the outer surface is considered. This can also be the reason why in the case of resin A the batch adsorption experiment shows a faster adsorption than the model is able to predict (more area is available for binding the same amount of VLPs).

Future studies will be conducted to obtain more accurate data on the batch uptake experiments using different detection methods such as MALS and NTA and different models will be tested.

6 References

[1] J. Fuenmayor, F. Gòdia, L. Cervera, Production of virus-like particles for vaccines, N. Biotechnol. 39 (2017) 174–180. doi:10.1016/j.nbt.2017.07.010.

[2] L.H.L. Lua, N.K. Connors, F. Sainsbury, Y.P. Chuan, N. Wibowo, A.P.J. Middelberg, Bioengineering virus-like particles as vaccines, Biotechnol. Bioeng. 111 (2014) 425–440. doi:10.1002/bit.25159.

[3] A.F. Rodrigues, H.R. Soares, M.R. Guerreiro, P.M. Alves, A.S. Coroadinha, Viral vaccines and their manufacturing cell substrates: New trends and designs in modern vaccinology, Biotechnol. J. 10 (2015) 1329–1344. doi:10.1002/biot.201400387.

[4] A. Roldao, M. Mellado, L. Castilho, M. Carrondo, P. Alves, Virus-like particles in vaccine development, Expert Rev Vaccines. 10 (2010) 1149–1176.

[5] D. Yan, Y.Q. Wei, H.C. Guo, S.Q. Sun, The application of virus-like particles as vaccines and biological vehicles, Appl. Microbiol. Biotechnol. 99 (2015) 10415–10432. doi:10.1007/s00253-015-7000-8.

[6] R.S. Felberbaum, The baculovirus expression vector system: A commercial manufacturing platform for viral vaccines and gene therapy vectors, Biotechnol. J. 10 (2015) 702–714. doi:10.1002/biot.201400438.

[7] F. Liu, X. Wu, L. Li, Z. Liu, Z. Wang, Use of baculovirus expression system for generation of virus-like particles: Successes and challenges, Protein Expr. Purif. 90 (2013) 104–116. doi:10.1016/j.pep.2013.05.00.

[8] R. Greco, M. Michel, D. Guetard, M. Cervantes-Gonzalez, N. Pelucchi, S. Wain-Hobson, F. Sala, M. Sala, Production of recombinant HIV-1/HBV virus-like particles in Nicotiana tabacum and Arabidopsis thaliana plants for a bivalent plant-based vaccine, Vaccine. 25 (2007) 8228–8240. doi:10.1016/j.vaccine.2007.09.061.

[9] Q. Chen, K.R. Davis, The potential of plants as a system for the development and production of human biologics, F1000Research. 5 (2016) 912. doi:10.12688/f1000research.8010.1.

[10] J. Zhu, Mammalian cell protein expression for biopharmaceutical production, Biotechnol. Adv. 30 (2012) 1158–1170. doi:10.1016/j.biotechadv.2011.08.022.

[11] L. Cervera, S. Gutiérrez-Granados, M. Martínez, J. Blanco, F. Gòdia, M.M. Segura, Generation of HIV-1 Gag VLPs by transient transfection of HEK 293 suspension cell cultures using an optimized animal-derived component free medium, J. Biotechnol. 166 (2013) 152–165. doi:10.1016/j.jbiotec.2013.05.001.

[12] M.G. Masavuli, D.K. Wijesundara, J. Torresi, E.J. Gowans, B. Grubor-Bauk, Preclinical Development and Production of Virus-Like Particles As Vaccine Candidates for Hepatitis C,

Front. Microbiol. 8 (2017) 1–11. doi:10.3389/fmicb.2017.02413.

[13] Y. Xiao, H.Y. Chen, Y. Wang, B. Yin, C. Lv, X. Mo, H. Yan, Y. Xuan, Y. Huang, W. Pang, X. Li, Y.A. Yuan, K. Tian, Large-scale production of foot-and-mouth disease virus (serotype Asia1) VLP vaccine in Escherichia coli and protection potency evaluation in cattle, BMC Biotechnol. 16 (2016). doi:10.1186/s12896-016-0285-6.

[14] P. Steppert, D. Burgstaller, M. Klausberger, P. Kramberger, A. Tover, E. Berger, K. Nöbauer, E. Razzazi-Fazeli, A. Jungbauer, Separation of HIV-1 gag virus-like particles from vesicular particles impurities by hydroxyl-functionalized monoliths, J. Sep. Sci. 40 (2017) 979–990. doi:10.1002/jssc.201600765.

[15] P. Steppert, D. Burgstaller, M. Klausberger, E. Berger, P.P. Aguilar, T.A. Schneider, P. Kramberger, A. Tover, K. Nöbauer, E. Razzazi-Fazeli, A. Jungbauer, Purification of HIV-1 gag virus-like particles and separation of other extracellular particles, J. Chromatogr. A. 1455 (2016) 93–101. doi:10.1016/j.chroma.2016.05.053.

[16] P. Nestola, C. Peixoto, R.R.J.S. Silva, P.M. Alves, J.P.B. Mota, M.J.T. Carrondo, Improved virus purification processes for vaccines and gene therapy, Biotechnol. Bioeng. 112 (2015) 843–857. doi:10.1002/bit.25545.

[17] M.W. Wolf, U. Reichl, Downstream processing of cell culture-derived virus particles, Expert Rev. Vaccines. 10 (2011) 1451–1475. doi:10.1586/erv.11.111.

[18] C.L. Effio, J. Hubbuch, Next generation vaccines and vectors: Designing downstream processes for recombinant protein-based virus-like particles, Biotechnol. J. 10 (2015) 715–727. doi:10.1002/biot.201400392.

[19] P. Steppert, D. Burgstaller, M. Klausberger, A. Tover, E. Berger, A. Jungbauer, Quantification and characterization of virus-like particles by size-exclusion chromatography and nanoparticle tracking analysis, J. Chromatogr. A. 1487 (2017) 89–99. doi:10.1016/j.chroma.2016.12.085.

[20] S.B. Carvalho, M.G. Moleirinho, D. Wheatley, J. Welsh, R. Gantier, P.M. Alves, C. Peixoto, M.J.T. Carrondo, Universal label-free in-process quantification of influenza virus-like particles, Biotechnol. J. 12 (2017). doi:10.1002/biot.201700031.

[21] P. Kramberger, L. Urbas, A. Štrancar, Downstream processing and chromatography based analytical methods for production of vaccines, gene therapy vectors, and bacteriophages, Hum. Vaccines Immunother. 11 (2015) 1010–1021. doi:10.1080/21645515.2015.1009817.

[22] T. Vicente, A. Roldão, C. Peixoto, M.J.T. Carrondo, P.M. Alves, Large-scale production and purification of VLP-based vaccines, J. Invertebr. Pathol. 107 (2011) S42–S48. doi:10.1016/j.jip.2011.05.004.

[23] Z. Jiang, G. Tong, B. Cai, Y. Xu, J. Lou, Purification and immunogenicity study of human papillomavirus 58 virus-like particles expressed in Pichia pastoris, Protein Expr. Purif. 80 (2011) 203–210. doi:10.1016/j.pep.2011.07.009.

[24] P.E. Cruz, C.C. Peixoto, K. Devos, J.L. Moreira, E. Saman, M.J.T. Carrondo, Characterization and downstream processing of HIV-1 core and virus-like- particles produced in serum free medium, Enzyme Microb. Technol. 26 (2000) 61–70. doi:10.1016/S0141-0229(99)00128-3.

[25] A. Jungbauer, Continuous downstream processing of biopharmaceuticals, Trends Biotechnol. 31 (2013) 479–492. doi:10.1016/j.tibtech.2013.05.011.

[26] A.A. Shukla, U. Gottschalk, Single-use disposable technologies for biopharmaceutical manufacturing, Trends Biotechnol. 31 (2013) 147–154. doi:10.1016/j.tibtech.2012.10.004.

[27] L. Besnard, V. Fabre, M. Fettig, E. Gousseinov, Y. Kawakami, N. Laroudie, C. Scanlan, P. Pattnaik, Clarification of vaccines: An overview of filter based technology trends and best practices, Elsevier B.V., 2016. doi:10.1016/j.biotechadv.2015.11.005.

[28] P. Gagnon, M.C. Flickinger, Chromatographic Purification of Virus Particles, Encycl. Ind. Biotechnol. m (2009). doi:10.1002/9780470054581.eib583.

[29] C. Charcosset, Ultrafiltration, in: Membr. Process. Biotechnol. Pharm., 2012: pp. 43–99. doi:10.1016/B978-0-444-56334-7.00002-2.

[30] T. Koho, T. Mäntylä, P. Laurinmäki, L. Huhti, S.J. Butcher, T. Vesikari, M.S. Kulomaa, V.P. Hytönen, Purification of norovirus-like particles (VLPs) by ion exchange chromatography, J. Virol. Methods. 181 (2012) 6–11. doi:10.1016/j.jviromet.2012.01.003.

[31] G. Carta, A. Jungbauer, Protein Chromatography: Process Development and Scale-Up, 2010. doi:10.1002/9783527630158.

[32] R. Hahn, A. Tscheliessnig, P. Bauerhansl, A. Jungbauer, Dispersion effects in preparative polymethacrylate monoliths operated in radial-flow columns, J. Biochem. Biophys. Methods. 70 (2007) 87–94. doi:10.1016/j.jbbm.2006.09.005.

[33] W.I. Sundquist, H.G. Kräusslich, HIV-1 assembly, budding, and maturation, Cold Spring Harb. Perspect. Med. 2 (2012) 1–24. doi:10.1101/cshperspect.a006924.

[34] C. Zhao, Z. Ao, X. Yao, Current Advances in Virus-Like Particles as a Vaccination Approach against HIV Infection, Vaccines. 4 (2016) 2. doi:10.3390/vaccines4010002.

[35] N.L. Goicochea, S.A.K. Datta, M. Ayaluru, C. Kao, A. Rein, B. Dragnea, Structure and stoichiometry of template-directed recombinant HIV-1 Gag particles, J. Mol. Biol. 410 (2011) 667–680. doi:10.1016/j.jmb.2011.04.012.

[36] B. Michen, T. Graule, Isoelectric points of viruses, J. Appl. Microbiol. 109 (2010) 388–397. doi:10.1111/j.1365-2672.2010.04663.x.

[37] R. Corbett, G. Carta, T. Iskra, C. Gallo, R. Godavarti, J.R. Salm, Structure and protein adsorption mechanisms of clean and fouled tentacle-type anion exchangers used in a monoclonal antibody polishing step, J. Chromatogr. A. 1278 (2013) 116–125. doi:10.1016/j.chroma.2013.01.006.

[38] S. Zhang, T. Iskra, W. Daniels, J. Salm, C. Gallo, R. Godavarti, G. Carta, Structural and performance characteristics of representative anion exchange resins used for weak partitioning chromatography, Biotechnol. Prog. 33 (2017) 425–434. doi:10.1002/btpr.2412.

[39] L. Hagel, M. Östberg, T. Andersson, Apparent pore size distributions of chromatography media, J. Chromatogr. A. 743 (1996) 33–42. doi:10.1016/0021-9673(96)00130-6.

[40] G. Carta, A.R. Ubiera, T.M. Pabst, Protein mass transfer kinetics in ion exchange media: Measurements and interpretations, Chem. Eng. Technol. 28 (2005) 1252–1264. doi:10.1002/ceat.200500122.

[41] P. DePhillips, A.M. Lenhoff, Pore size distributions of cation-exchange adsorbents determined by inverse size-exclusion chromatography, J. Chromatogr. A. 883 (2000) 39–54. doi:10.1016/S0021-9673(00)00420-9.

7 Acknowledgments

I would like to thank Professor Giorgio Carta for hosting me in his laboratory, for all the interesting discussions and all the shared knowledge. Moreover, I would like to thank all his students (Yiran Wang, Arch Creasy, Jason Reck, Preston Fuks, Lukas Kimerer, Joey Roberts and Andreas Alberti) for the help in the laboratory, the knowledge sharing, the happy hours, dinners, concerts… for their great hospitality in general. You all made my stay abroad a special and unforgettable time.

Thank you!